Peculiar features of nuclear resonant Bragg scattering

G. V. Smirnov[1,*] and A. I. Chumakov [2,1]

[1]*National Research Center "Kurchatov Institute," 123182 Moscow, Russia*
[2]*ESRF-The European Synchrotron, CS40220 38043 Grenoble Cedex 9, France*

The properties of x-ray diffraction are compared for two principally different scattering mechanisms: potential and resonant. The first mechanism is well represented by elastic scattering from atomic electrons (Rayleigh scattering), while the second one is offered by recoilless resonant scattering from nuclei (Mössbauer scattering). Diffraction in Bragg geometry from a semi-infinite crystal is considered. Mainly, the spatial aspects of scattering are discussed like angular dependencies, distributions of electric and magnetic fields inside the crystal and, especially, the role of asymmetry in the diffraction geometry. The results of the model calculations are presented for a complex reflection coefficient, for total wave fields and their interaction with atoms, for path lengths in transmission of radiation through the crystal, and for an interplay between absorption and reflection of radiation by the atomic ensemble.

I. PRELIMINARY COMMENTS

A long time passed after the discovery of x-ray diffraction [1] predicted by von Laue before the diffraction of resonant γ radiation by nuclear crystal lattice was observed [2]. Much earlier than this observation, several successful attempts were made to excite radiative nuclear transitions with use of electromagnetic radiation, but nobody at that time had regarded the feasibility of nuclear diffraction because of an assumed violation of the wave coherence, which was expected due to a recoil during an absorption and emission of γ-ray photon by the nuclei. Only after the discovery of the recoilless nuclear resonance fluorescence by Mössbauer [3], such a possibility started to be considered as real. The recoilless mechanism ensures the existence in crystals of the nuclear resonance of natural width and the possibility of emission by nuclei of γ-ray photons having a record coherence length. It is amazing that the wave packet of a Mössbauer γ quantum can contain, for instance, $\sim 10^{11}$ or $\sim 10^{13}$ unperturbed oscillations for nuclear transitions in the ^{57}Fe and ^{67}Zn isotopes, respectively.

An ensemble of Mössbauer nuclei in a crystal could represent for electromagnetic radiation a resonating diffraction grating. The interaction of γ-ray photons with nuclei is a case of resonance scattering, where the nucleus presents a perfect two-level system. The entire process of scattering can be divided into three stages: an absorption of a primary quantum with formation of an intermediate excited state, dwelling in the intermediate state, usually a long-lived one, and a transition back to the ground state with emission of a secondary particle. Concerning the creation of the excited state, there could not be any doubt that the energy of a γ-ray photon is sufficient to excite only a single nucleus. Seemingly, the described picture of the scattering process makes it tempting to consider the interaction in terms of localization. On the other hand, observation of such a collective phenomenon like diffraction would mean that all nuclei in a scattering ensemble must be touched by excitation. So, the critical question was *how one could imagine a collective excitation in an ensemble of nuclei, if the photon energy is sufficient to excite only one nucleus.*

In order to resolve this contradiction, the idea of the delocalized nuclear excitation was introduced by Trammell [4] and Kagan and Afanas'ev [5]. Within this idea, in the absence of an indication which nucleus is excited, each one should be considered as excited with the *definite probability amplitude* in accordance with the quantum-mechanical principle of superposition of states. Such a delocalized excitation has been called a nuclear exciton. If the state where one nucleus is excited and all other nuclei are in the ground state is an elementary state of excitation, then, in this model, the nuclear exciton wave function is a linear superposition of such elementary excitations. Thus, the nuclear excitation is delocalized, and a photon is shared by all nuclei. This is how the scattering process exhibits a collective character. *By these features of nuclear excitation, the resonance diffraction of a γ-ray photon from an ensemble of nuclei should be considered as a macroscopic quantum phenomenon. The crystal behaves in the photon diffraction process as a macroscopic quantum-mechanical object, the macroscopic quantum resonator.*

The existence of nuclear exciton provides the physical basis for the use of a macroscopic polarization given by the Maxwell equations to treat the radiative effects of nuclei. The macroscopic polarization of a nuclear ensemble is the sum of the induced nuclear transition moments over a unit volume, i.e., the density of the induced electric or magnetic moment, depending on the multipolarity of the nuclear transition. It represents a quantum-mechanical average over the nuclear ensemble.

A number of features distinguishes the elementary acts of interaction of resonant and nonresonant radiation with an

---

*g.smirnov@gmx.net

TABLE I. Specific features of scattering.

	In resonance	Off resonance
Scattering mechanism in the wavelength range $\sim 0.5-1.5$Å	Resonant nuclear+ potential electronic	Dominant potential+ weak resonant+ weak Compton
Temporal aspects	Long-lived intermediate nuclear state $\sim 10^{-5}$–10^{-9}s	Fast collision $\sim 10^{-17}$s
Elastic and inelastic scattering channels	(γ, γ) and (γ, e^-) inelastic (γ, e^-) is dominant	(x, x) and (x, e^-) elastic (x, x) is dominant
Intra-atomic interference	Nuclear radius $r_n \ll \lambda$ no form factor	Atomic radius $r_a \sim \lambda$ a big role of form factor
Multipolarity of transition	Clear-cut nuclear transition multipoles $E1$ or $M1(+)E2$	Hierarchy of multipoles $E1, M1, E2$
Polarization dependence	Complex in presence of hyperfine splitting. Optical activity of media is essential	Specific for $E1$ transition

atom. Some of them are listed in Table I. An interaction of x rays with electrons in atoms is dominated by Rayleigh scattering. A resonant contribution to the electronic scattering amplitude plays the role of a slight perturbation which, however, in special applications may be important. On the contrary, the interaction of x rays with atomic nuclei is the case of pure resonance scattering characterized by the narrow resonances and, therefore, it is highly sensitive to the frequency deviation from the resonant frequency. The principal difference mentioned above concerns the duration of the scattering process: 10^{-5}–10^{-9} s for nuclear resonant scattering versus 10^{-17} s for electronic nonresonant scattering.

Another important difference is related to a significance of an elastic radiative channel of scattering. As Table I shows, the radiative channel is dominant for electronic scattering, but plays a minor role for the low-energy nuclear isomeric transition. The probability of an internal electronic conversion in scattering at an individual nucleus is so large that a localization of excitation with a loss of a photon is very likely. And yet the *coherence in the collective response of nuclei* in a crystal permits the radiative channel not only to survive, but even to become dominant in the process of interaction of a γ-ray photon with a nuclear array. Due to the constructive contributions of all scattering paths, the *probability of γ-ray reemission is strongly enhanced*. Under the conditions where the radiationless process (internal electronic conversion) is dominant in the interaction with an isolated nucleus, this *enhancement effect is of great importance for the survival of a γ ray in a large nuclear ensemble*.

Among other peculiar features one should note the absence of destructive interference in scattering from a nucleus because of the negligible size of nuclear radius in comparison to the wavelength of radiation. Therefore, nuclear form factor in the scattering amplitude is always equal to unity, independently of the scattering angle. Another feature of nuclear resonant scattering is related to the possibility of hyperfine interaction, which arises in the presence of internal electric or magnetic crystalline fields. Due to this, the nuclear ensemble represents in general an optically active medium.

Various wave field configurations can be constructed by using a polarization-dependent selective excitation of nuclear transitions under conditions of their hyperfine splitting.

Experiments where diffraction of electromagnetic waves by a nuclei array in a crystalline lattice has been observed gave convincing evidence of a full space-time coherence in nuclear resonance scattering. The existence of nuclear diffraction clearly proved the possibility of coherent radiative coupling of nuclear oscillators, which was spread over the crystal volume with the dimensions very large in comparison to the wavelength, and during extremely long times characterized by the lifetime of nuclear excited state. The total field in the crystal represents a coherent superposition of waves "allowed" by scattering system, i.e., the waves that are eigensolutions of the Maxwell equations of the scattering problem.

Potential scattering is characterized by an amplitude independent of radiation frequency, and it is practically a real value. Such kind of scattering is realized in the process of elastic scattering far away from an absorption edge. On the contrary, resonant scattering is characterized by the amplitude sharply dependent on the radiation frequency. Strictly in resonance, it is a pure imaginary value.

In the simulation of electronic and nuclear scattering of x rays in a crystal, we assume that atoms are frozen and no atomic motions occur, i.e., that the Debye-Waller factor, accounting for thermal vibrations of atoms in a potential scattering, and the Lamb-Mössbauer factor, accounting for thermal vibrations of nuclei in resonance scattering, are equal to unity. This assumption will not affect the physical results within the framework of the task of our article.

We discuss mainly the spatial aspects of scattering like angular dependencies, distributions of electric and magnetic fields inside the crystal and, especially, the role of asymmetry in the diffraction geometry. The energy dependence of the nuclear resonance scattering has been extensively studied in a number of experiments (see, e.g., overview in [6]). Therefore, it is not discussed in this paper.

In order to outline the theoretical basis of the paper, in Sec. II the elements of the dynamical diffraction theory are

given in the application to the case of Bragg scattering from a semi-infinite crystal. Then, in Sec. III a comparison of electronic and nuclear diffraction in model calculations is presented. In Sec. IV, the role of asymmetry in the geometry of scattering is considered. Finally, some concluding remarks are provided.

II. ELEMENTS OF THE THEORY

A. Solution for the reflection in Bragg geometry

The simplest and most fundamental electromagnetic waves are transverse plane waves. The theory of stationary scattering describes the transformation of a plane wave of electromagnetic radiation due to its interaction with atoms. A transverse plane electromagnetic wave is characterized by the frequency of radiation ω, by the wave vector $\mathbf{k}$, and by the polarization vector $\mathbf{e}$. The frequency is related to the radiation energy $E = \hbar\omega$. The wave vector is normal to the wave front, and its absolute value, or the circular wave number is determined by the wavelength of radiation $K = 2\pi/\lambda$. The polarization vector $\mathbf{e}$ is represented by the unit vector normal to the wave vector. The state of radiation is significantly modified due to interaction with atoms in substance. The excited atomic currents contribute to the field, and the constructive interference of the waves emitted by atoms gives rise to the formation of the strong waves in some directions when the Bragg requirements are satisfied. We suppose that Bragg reflection can occur only from one set of atomic planes in a crystal. In this case, two strong waves are generated in the crystal: the wave propagating in the forward direction with the wave vector $\mathbf{k}_0$, and the diffracted wave with the wave vector $\mathbf{k}_1 = \mathbf{k}_0 + \mathbf{S}$, where $\mathbf{S}$ is the scattering vector. The vectors $\mathbf{k}_0$ and $\mathbf{k}_1$ form the scattering plane. The scheme of the two-wave diffraction is represented in Fig. 1.

Linearly polarized electromagnetic wave is described by a combination of two mutually orthogonal polarization states σ and π. The unit vectors of the incident and scattered σ-polarized waves $\mathbf{e}_{0,1}^\sigma$ are determined by the vector products $\mathbf{e}_{0,1}^\sigma = [\mathbf{k}_1 \times \mathbf{k}_0]/|[\mathbf{k}_1 \times \mathbf{k}_0]|$. They are normal to the scattering plane. The unit vectors of the π-polarized waves $\mathbf{e}_{0,1}^\pi$ are determined by the vector products $\mathbf{e}_{0,1}^\pi = [\mathbf{k}_{0,1} \times \mathbf{e}_{0,1}^\sigma]/K$, both lying in the scattering plane. The oscillation of the electric field strength in the wave goes along the polarization vector $\mathbf{e}$, while the oscillation of the magnetic field strength in the wave goes along the polarization vector $\mathbf{h}$. The latter is determined as $\mathbf{h}_d^s = [\mathbf{k}_d \times \mathbf{e}_d^s]/K$, where s and d are the polarization and the direction indices.

The dynamic theory takes into account multiple scattering of radiation in the crystal. In a steady state, the dynamical equilibrium in the exchange of energy between the radiation field and the excited atomic currents is established due to multiple scattering. As a result, the total field in the crystal represents a coherent superposition of the waves allowed by the scattering system. These waves are dynamically coupled via atomic currents feeding each other so that the total field must be considered as a single entity [7]. As mentioned above, here we limit ourselves to considering the case where two waves are formed due multiple scattering: the wave propagating in a direction close to the primary one and the diffracted wave.
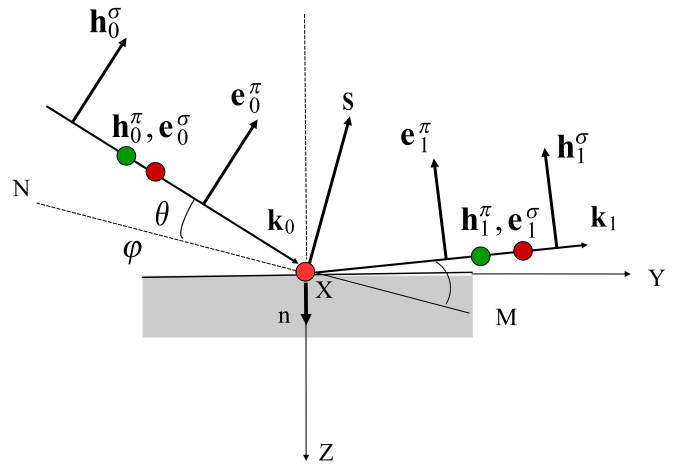
FIG. 1. The scattering scheme is presented in the XYZ rectangular coordinate system. The crystal surface lies in the XY plane. In the Bragg reflection geometry, the incident and the reflected waves are located above the crystal surface. The wave vectors $\mathbf{k}_0$ and $\mathbf{k}_1$ describe the waves propagating through the crystal in the forward and the reflection directions, respectively. The incident wave can be either σ or π polarized. The electric polarization vectors $\mathbf{e}_0^\sigma$, $\mathbf{e}_1^\sigma$ and the magnetic polarization vectors $\mathbf{h}_0^\pi$, $\mathbf{h}_1^\pi$ are normal to the scattering plane, the direction from the observer is given in red (dark gray), while that toward the observer in green (light gray), the electric vectors $\mathbf{e}_0^\pi$, $\mathbf{e}_1^\pi$ and the magnetic vectors $\mathbf{h}_0^\sigma$, $\mathbf{h}_1^\sigma$ lie in the scattering plane, vector $\mathbf{S} = \mathbf{k}_1 - \mathbf{k}_0$ is the scattering vector, $\mathbf{n}$ is the unit vector in the direction of the inward normal to the crystal surface. The reflecting planes are orthogonal to the plane of figure and inclined to the crystal surface at angle φ, NM is the trace of a reflecting plane, θ is the angle between the incident beam and reflecting plane.

In Fig. 1 the asymmetric diffraction geometry is displayed, where the glancing angle of incidence $\theta_0 = \theta + \varphi$ is greater than the glancing angle of reflection $\theta_1 = \theta - \varphi$. The asymmetry factor β characterizing the geometry of scattering is determined by the ratio of scalar products of the wave vectors of the incident and diffracted waves and the unit vector $\mathbf{n}$, directed along the inward normal to the crystal surface, $\beta = (\mathbf{n}\mathbf{k}_0)/(\mathbf{n}\mathbf{k}_1)$. Using Fig. 1 to determine the asymmetry factor, we obtain $\beta = -\sin\theta_0/\sin\theta_1$. For the geometry displayed in Fig. 1, the asymmetry factor $|\beta| > 1$. We shall call this case a steep incidence. In the reverse course of the rays, $|\beta| < 1$, the case will be called a grazing incidence. In the symmetric geometry angle $\varphi = 0$ and $\beta = -1$.

Solving the dynamical equations for the reflection from only one set planes in a semi-infinite crystal, one arrives at the following expression for the wave field inside the crystal [8,9]:

$$\mathbf{E}(\mathbf{r}) = \exp(i\mathbf{K}\mathbf{r})\exp\left(-iK\varepsilon_0^{(2)}L\right)$$

$$\times E_0\left[\mathbf{e}_0 - \frac{\beta\tilde{\eta}_{10}}{2\varepsilon_0^{(1)} - \tilde{\eta}_{00}}\mathbf{e}_1\exp\left(i\mathbf{S}\mathbf{r}\right)\right], \qquad (1)$$

where $\mathbf{K}$ is the wave vector of radiation in free space, $\mathbf{r}$ is the vector from the origin of coordinates to the observation point, L is the path length of radiation in the crystal to the point of observation, i.e., the projection of $\mathbf{r}$ vector on the direction of incidence. In Eq. (1), E_0 is the scalar amplitude of the incident

wave, $\varepsilon_0^{(1,2)}$ are small complex values showing the deviation of the refractive index from unity. They are determined as

$$\varepsilon_0^{(1,2)} = \tfrac{1}{4}\big\{\widetilde{\eta}_{00} + \beta\widetilde{\eta}_{11} - \alpha\beta$$
$$\mp \sqrt{(\widetilde{\eta}_{00} - \beta\widetilde{\eta}_{11} + \alpha\beta)^2 + 4\beta\widetilde{\eta}_{01}\widetilde{\eta}_{10}}\big\}, \quad (2)$$

parameters $\widetilde{\eta}_{dd'}$ represent the Fourier coefficients in the expansion of the crystal susceptibility in **S** space, i.e., in the space of scattering vectors. Parameter α in Eq. (2) is related to the deviation of the wave vector of the incident wave from the direction determined by the Bragg condition: $\Delta\theta = \theta - \theta_B$, $\alpha = -2\sin 2\theta_B \Delta\theta$, where θ_B is the Bragg angle. In the following, we call parameters $\widetilde{\eta}_{dd'}$ briefly as susceptibilities of the crystal. *A susceptibility is actually determined by the amplitude of scattering from the crystal unit cell.* The scattering amplitude is a complex function that relates amplitudes, phases, and polarizations of the spectral components of the incident and the reflected radiation. Near the resonance energy, the susceptibility of the crystal containing resonant nuclei includes both the electronic and the nuclear contributions, correspondingly, $\widetilde{\eta} = \chi + \eta$. Below, we shall analyze the cases where polarization does not change in scattering, therefore, the polarization indices will be omitted. Indices dd' indicate the directions of propagation of the waves in the case of two-wave diffraction; d, $d' = 0, 1$. When polarization of the waves does not change, the set of susceptibilities $\widetilde{\eta}_{dd'}$ represents the matrix of second rank, where each element is proportional to the amplitude of scattering from one permitted direction to the other: $0 \to 0$, $0 \to 1$, $1 \to 0$, and $1 \to 1$. The structure of the electronic and the nuclear susceptibilities will be regarded in the next subsection.

The first term in Eq. (1) represents the wave propagating through the crystal near the direction of the primary wave, while the second term represents the diffracted wave. The complex amplitude of the diffracted wave contains an additional phase factor $\exp(i\mathbf{Sr})$, originating due to diffraction of radiation in the crystal, the scattering vector **S** is orthogonal to the reflecting planes. The additional phase is defined by the projection of vector **r** on the direction of **S** vector. When the condition for Bragg scattering is fulfilled, $|\mathbf{S}| = 2\pi/D$, where D is the distance between the neighboring reflecting planes. Let $\mathbf{r}_m$ and $\mathbf{r}_{m+1}$ be the vectors to the observation points at the neighboring reflecting planes. The projection of the vectors' difference on the direction of **S** is equal to D. Thus, the spatial phase changes by 2π in shifting of the observation point from an arbitrary chosen reflecting plane to the neighboring one. As a result of summation of the propagating and the diffracted waves, the amplitude of the total electromagnetic field in the crystal is spatially modulated in the direction orthogonal to the reflecting planes. Yet, we turn back to this issue later. Under conditions of the constructive interference, the phase factor $\exp(i\mathbf{Sr}_m) = 1$, and for the field amplitude in the case $\mathbf{e}_0 = \mathbf{e}_1$ we obtain

$$E(L) = \exp\left(-iK\varepsilon_0^{(2)}L\right)E_0\left[1 - \frac{\beta\widetilde{\eta}_{10}}{2\varepsilon_0^{(1)} - \widetilde{\eta}_{00}}\right]. \quad (3)$$

For this case, in the nearest vicinity to the reflecting plane m, *regardless of the depth of its location in the crystal*, the ratio

of the scalar amplitudes of the scattered and the propagating waves E_1/E_0 is

$$R = -\frac{\beta\widetilde{\eta}_{10}}{2\varepsilon_0^{(1)} - \widetilde{\eta}_{00}}; \quad (4)$$

this ratio represents the reflection coefficient. Another important characteristic of the coherent Bragg scattering is the reflectivity of a crystal, which describes the scattering in the terms of the energy fluxes. The latter is represented by the product $W = IS$ of the radiation intensity I and radiation beam cross section S. The reflectivity Q is given by the ratio W_1/W_0 of the energy flux in the reflected beam to that in the incident one. Finally, using the definition for the reflection coefficient and taking into account that the ratio $S_0/S_1 = |\beta|$, we obtain for the reflectivity

$$Q = |R|^2\frac{1}{|\beta|}. \quad (5)$$

In the following, we analyze the characteristic features of the wave field in crystal described by Eq. (1) for two types of interaction of radiation with atoms. As a thought experiment, we shall consider the diffraction of radiation in the crystal of iron consisting completely of the nuclear resonant isotope ^{57}Fe. The crystal of iron in alpha phase has a cubic lattice with the lattice constant of 2.866 Å. The unit cell of iron contains two iron atoms: one of them is located in the cube corner and another one in the center of cube.

Concerning an interaction with nuclei, we shall consider the transition between the ground and the first excited states of ^{57}Fe with the energy of 14.41 keV. The spin of ^{57}Fe nucleus is equal to $\frac{1}{2}$ in the ground state and $\frac{3}{2}$ in the excited state. Therefore, in the interaction of radiation with the nuclei, the magnetic dipole transition $M1$ is excited. Because iron is a ferromagnet, the local magnetic fields at iron nuclei cause hyperfine splitting of nuclear levels both in the ground and in the excited states.

B. Electronic and nuclear susceptibility of the crystal

For comparison of modes of electronic and nuclear scattering, we explore one and the same case of permitted Bragg reflection. Let the crystal be cut in such a way that the crystalline planes $(00n)$ are orthogonal to the YZ plane, as shown in Fig. 1. The first structurally allowed reflection from this set of planes is the (002) reflection. The Bragg angle of this reflection for radiation with the energy of 14.41 keV is $\theta_B = 17.47°$. An interaction with electrons of atomic shells is characterized by the same amplitude at any frequency of the incident radiation in the range of nuclear γ resonance. The electronic oscillations of different multipolarity are excited. However, among the excited multipoles there is a significant hierarchy, where the dominant role belongs to the electric dipole oscillation $E1$.

For the electronic susceptibility, we use the expression from the theory of x-ray scattering (see, e.g., [10])

$$\chi_{dd'}^{ss'} = \big(\mathbf{e}_d^s\mathbf{e}_{d'}^{s'}\big)\frac{\lambda^2}{\pi V_0}\sum_{a=1,2}\left[-r_0 f_a(\mathbf{k}_{d'} - \mathbf{k}_d) - i\frac{1}{2\lambda}\sigma_a^{\mathrm{ph}}\right]$$
$$\times \exp\{-i(\mathbf{k}_{d'} - \mathbf{k}_d)\mathbf{r}_a\}\exp\{-W_a(\mathbf{k}_{d'} - \mathbf{k}_d)\}, \quad (6)$$

TABLE II. The susceptibility of iron crystal for reflection (002).

Electronic	Nuclear $-\frac{1}{2} \Rightarrow -\frac{1}{2}$	Nuclear $-\frac{1}{2} \Rightarrow -\frac{3}{2}$
$\begin{Bmatrix} \chi_{00} & \chi_{01} \\ \chi_{10} & \chi_{11} \end{Bmatrix}$	$\begin{Bmatrix} \eta_{00}^{\pi\pi} & \eta_{01}^{\pi\pi} \\ \eta_{10}^{\pi\pi} & \eta_{11}^{\pi\pi} \end{Bmatrix}$	$\begin{Bmatrix} \eta_{00}^{\sigma\sigma} & \eta_{01}^{\sigma\sigma} \\ \eta_{10}^{\sigma\sigma} & \eta_{11}^{\sigma\sigma} \end{Bmatrix}$
$\begin{Bmatrix} \mathrm{Re}\chi_{00} + i\,\mathrm{Im}\chi & \mathrm{Re}\chi_{01} + i\,\mathrm{Im}\chi \\ \mathrm{Re}\chi_{10} + i\,\mathrm{Im}\chi & \mathrm{Re}\chi_{11} + i\,\mathrm{Im}\chi \end{Bmatrix}$	$-i\eta^{\pi\pi}\begin{Bmatrix} 1 & 1 \\ 1 & 1 \end{Bmatrix}$	$-i\eta^{\sigma\sigma}\begin{Bmatrix} 1 & \exp(+i2\theta_B) \\ \exp(-i2\theta_B) & 1 \end{Bmatrix}$

$$\mathrm{Re}\chi_{00} = \mathrm{Re}\chi_{11} = -14.56, \ \mathrm{Re}\chi_{01}^{\sigma\sigma} = \mathrm{Re}\chi_{10}^{\sigma\sigma} = -8.54, \ \mathrm{Im}\chi^{\sigma\sigma} = -0.66 \ (\text{in units } 10^{-6})$$

$$\mathrm{Re}\chi_{01}^{\pi\pi} = \mathrm{Re}\chi_{10}^{\pi\pi} = -7.0, \ \mathrm{Im}\chi^{\pi\pi} = -0.54, \ \eta^{\pi\pi} = 143.34, \ \eta^{\sigma\sigma} = 107.51 \ (\text{in units } 10^{-6})$$

where the outer brackets represent the polarization factor, V_0 the unit-cell volume, r_0 classical electron radius, f_a the atomic form factor, depending on the scattering angle (dispersion correction Δf_a to the atomic factor is omitted here), σ_a^{ph} the photoeffect cross section, $\mathbf{r}_a$ the coordinate of atom in the unit cell of crystal, $\exp(-W_a)$ the Debye-Waller factor, the summation is carried out over the atoms of the unit cell. For the crystal of α iron, $V_0 = 23.54 \ \mathrm{\mathring{A}}^3$. In the definition of electronic susceptibility, the real part is negative in consistence with the phase shift of $-\pi$, which should hold for the wave scattered much above the K edge. A negative sign before the imaginary part is associated with the choice of sign in the exponential index $\exp(-i\kappa\varepsilon_0^{(2)}z/\sin\theta_0)$. With such a choice of the sign, the physical condition of absorption of radiation in the crystal is satisfied.

When the σ-polarized wave is incident on the crystal, the polarization factor $(\mathbf{e}_d^\sigma \mathbf{e}_{d'}^\sigma) \equiv 1$ (see Fig. 1). In the absence of thermal motions, $\exp(-W_a) \equiv 1$. In the calculations using Eq. (6), the following values of the physical quantities were used: $r_0 = 2.82 \times 10^{-13}$ cm, $\sigma_{\mathrm{Fe}}^{\mathrm{ph}} = 0.57 \times 10^{-20}$ cm^2, $f_a(0) = 26$, $f_a(2\theta_B^{(002)}) = 15.25$, $\exp\{-i(\mathbf{k}_{d'} - \mathbf{k}_d)\mathbf{r}_a\}_{(002)} = 1$. The susceptibility matrix for electronic scattering is shown in the left column of Table II.

We turn to the nuclear susceptibility. Nucleus is a quantum-mechanical physical system. Therefore, the amplitudes of nuclear resonance scattering are calculated on the basis of quantum mechanics. With the electromagnetic field of the suitable frequency, the nuclear transition current is excited, which represents an oscillating multipole, in our case the magnetic dipole $M1$. The excited current determines directly the scattering amplitude. The latter is calculated as the quantum-mechanical average over the nuclear array in the crystal.

Due to the interaction of the internal magnetic field with the magnetic moments of nuclei in the ground and in the excited states, the energy levels in these states are split: in the ground state into two sublevels with the projections of the nuclear spin on the magnetic field of $+\frac{1}{2}$ and $-\frac{1}{2}$, and in the excited state into four sublevels with the spin projections of $-\frac{3}{2}, -\frac{1}{2}, +\frac{1}{2} +\frac{3}{2}$.

The matrix of the nuclear susceptibility has been calculated on the basis of the theory of nuclear resonance coherent scattering [11] in application to the nuclear diffraction in a crystal of iron [12]. The resonance structure of nuclear scattering is characterized by the factor $1/(E - E_{eg} - i)$, where E_{eg} is the energy of the transition between the ground and the excited states, and E is the energy of the incident radiation in units of $\Gamma/2$ with Γ being the width at half-height of resonance.

Assuming that the energy of incident radiation is equal to the resonance energy of the transition between specific sublevels of the ground and the excited states, we obtain

$$\eta_{dd'}^{ss'}(E = E_{eg})$$
$$= -i\frac{3}{KV_0}\sigma_0 \langle j_g, m_g; L, M | j_e, m_e \rangle^2 \sum_{a=1,2} \left(\mathbf{h}_d^s \mathbf{n}_{-M}^a\right)\left(\mathbf{h}_{d'}^{s'} \mathbf{n}_{-M'}^a\right)^*$$
$$\times \exp\{-i(\mathbf{k}_{d'} - \mathbf{k}_d)\mathbf{r}_a\} f_a^{\mathrm{LM}}(\mathbf{k}_d) f_a^{\mathrm{LM}}(\mathbf{k}_{d'}), \quad (7)$$

where the summation is taken over the nuclei of the unit cell, σ_0 the nuclear resonance cross section; $\langle j_g, m_g; L, M | j_e, m_e \rangle$ the Clebsch-Gordan coefficient for the electromagnetic transition of the multipolarity L between the ground and the excited states of nucleus, j_g, j_e the nuclear spin, and m_g, m_e the spin projections in the ground and the excited states, respectively, $M = m_e - m_g$ takes the values $0, \pm 1$, $(\mathbf{h}_d^s \mathbf{n}_{-M}^a)(\mathbf{h}_{d'}^{s'} \mathbf{n}_{-M'}^a)^*$ the polarization factor of nuclear resonance scattering when a specific transition between the components of hyperfine structure of the ground and the excited states is induced, $\mathbf{h}_d^s$, $\mathbf{h}_{d'}^{s'}$ the unit vectors of the magnetic polarization of the incident and the scattered waves, and $\mathbf{n}_{-M}^a$, $\mathbf{n}_{-M'}^a$ mutually orthogonal unit vectors, which define the spatial properties of the magnetic moment of nuclear transition, $f_a^{\mathrm{LM}}(\mathbf{k}_d) f_a^{\mathrm{LM}}(\mathbf{k}_{d'})$ the Lamb-Mössbauer factors which are equal to unity in the absence of thermal vibrations. In further calculations, the cross section of nuclear resonance scattering was taken equal to $\sigma_0 = 2.464 \times 10^{-18}$ cm^2.

The axes of easy magnetization in an iron crystal are directed along the edges of the cubic unit cell. Let the sample under study be oriented in a such way that the X axis coincides with the direction [100], as it is shown in Fig. 1, and the crystal is magnetized along this direction. For this orientation of the magnetic field at the nuclei, the orthogonal unit vectors take the following form: $\mathbf{n}_{\pm 1} = \mp\frac{1}{\sqrt{2}}(\mathbf{n}_y \pm i\mathbf{n}_z)$ and $\mathbf{n}_0 = \mathbf{n}_x$.

When the π-polarized wave is incident on the crystal as shown in Fig. 1, the magnetic polarization vector is oriented along the X axis. Then, the polarization factor of the scattering amplitude is nonzero only for nuclear transitions $-\frac{1}{2} \to -\frac{1}{2}$ and $+\frac{1}{2} \to +\frac{1}{2}$, i.e., out of six permitted transitions only two (with $M = 0$) are able to contribute to the scattering picture. For these transitions, we get $(\mathbf{h}_d^\pi \mathbf{n}_{-M}^a)(\mathbf{h}_{d'}^\pi \mathbf{n}_{-M'}^a)^* = 1$ and $\langle \frac{1}{2}, \pm\frac{1}{2}; 1, 0 | \frac{3}{2}, \pm\frac{1}{2} \rangle^2 = \frac{1}{6}$. We will analyze the diffraction picture for an isolated nuclear transition $-\frac{1}{2} \to -\frac{1}{2}$. The susceptibility matrix for this transition is given in the middle column of Table II.
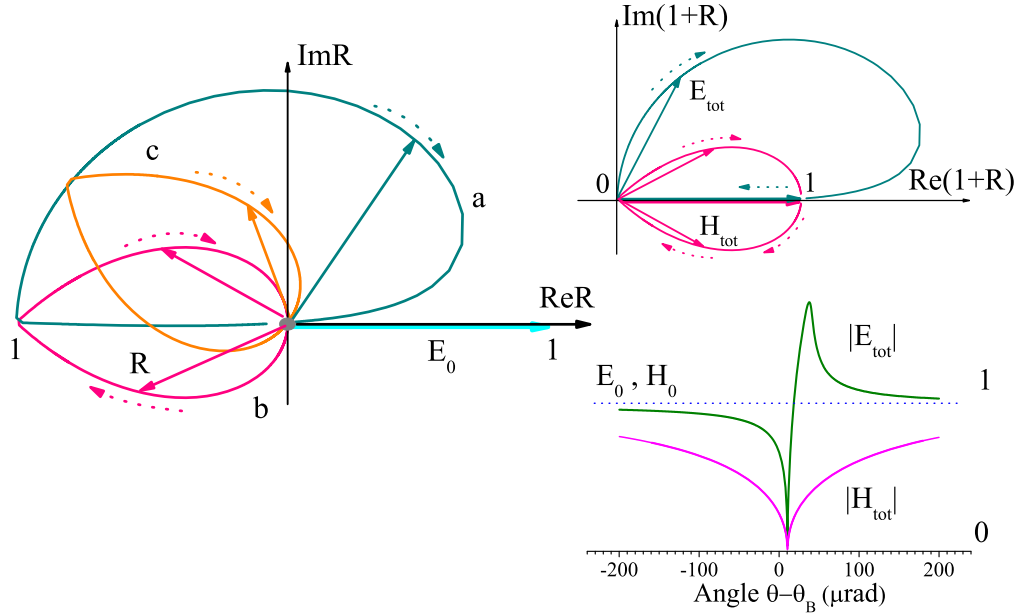
FIG. 2. Left panel: the angular dependencies of the reflection coefficient on the complex plane for potential electronic scattering (R contour a) and nuclear resonant scattering (R contours b and c for excitations of the $-\frac{1}{2} \rightarrow -\frac{1}{2}$ and $-\frac{1}{2} \rightarrow -\frac{3}{2}$ transitions, respectively). The bold arrow represents the unit vector with the phase of the incident wave, taken here for zero. Right panels: the angular dependencies of the total field amplitudes E_{tot} and H_{tot} at an arbitrary atomic reflecting plane: the complex values of the amplitudes (upper right panel), and the absolute values of the amplitudes (lower right panel) in electronic and nuclear scattering for the $-\frac{1}{2} \rightarrow -\frac{1}{2}$ transition. E_0, H_0 are the scalar amplitudes of electric and magnetic fields in the incident wave taken equal to unity.

When the σ-polarized wave is incident on the crystal, the magnetic polarization vector lies in the scattering plane YZ. In this case, the magnetic polarization vector is nonzero only for nuclear transitions $-\frac{1}{2} \rightarrow -\frac{3}{2}$, $-\frac{1}{2} \rightarrow +\frac{1}{2}$, $+\frac{1}{2} \rightarrow -\frac{1}{2}$, and $+\frac{1}{2} \rightarrow +\frac{3}{2}$, i.e., only the transitions having $M = \pm 1$ are able to contribute to the diffraction pattern. We will investigate the diffraction characteristics for an isolated nuclear transition $-\frac{1}{2} \rightarrow -\frac{3}{2}$. The polarization factors corresponding to this transition are equal $(\mathbf{h}_{0,1}^{\sigma} \mathbf{n}_1^a)(\mathbf{h}_{0,1}^{\sigma} \mathbf{n}_1^a)^* = 1$ and $(\mathbf{h}_{0,1}^{\sigma} \mathbf{n}_1^a)(\mathbf{h}_{1,0}^{\sigma} \mathbf{n}_1^a)^* = \exp(\pm i2\theta)$. The susceptibility matrix for this transition is given in the right column of Table II.

Upon an excitation of the transition $-\frac{1}{2} \rightarrow -\frac{1}{2}$, the matrix elements of the nuclear susceptibility are pure imaginary numbers, what corresponds to the wave phase shift of $-\pi/2$ for scattering exactly at resonance. Far away from a nuclear resonance, the incident radiation interacts only with electrons in the crystal. In this case, in calculations we will use the matrix of electronic susceptibility presented in Table II. If the radiation frequency coincides with the energy of nuclear transition, we will use the total matrix of the electronic and the nuclear susceptibilities, where, as it is easy to see from Table II, the nuclear part plays the dominant role.

III. COMPARISON OF ELECTRONIC AND NUCLEAR DIFFRACTION IN MODEL CALCULATION

A. Complex reflection coefficient

As discussed above, the reflection coefficient defined by Eq. (4) describes the amplitude and phase of the reflected wave relative to the corresponding parameters of the incident (propagating) wave at the position of reflecting plane,

regardless of its depth location in the crystal. The angular dependencies of the reflection coefficient are displayed on the complex plane in the coordinates ReR, ImR at the left-hand side of Fig. 2. The reflection coefficient at the fixed angle of incidence is represented by a vector R on this plane. Each of the closed contours on the plane is the locus of the R-vector end points corresponding either to electronic or nuclear scattering for variable scattering angle. We will call them R contours. Here, we assume symmetric Bragg scattering geometry, i.e., $\varphi = 0$ and $\beta = -1$.

The incidence angle changes in the angular range from $\theta \ll \theta_B$ to $\theta \gg \theta_B$. At large deviations from the Bragg angle, the angular parameter $\alpha \gg \tilde{\eta}_{00}$, so that $R \approx |\beta| \tilde{\eta}_{10}/\alpha$. Accordingly, the initial phase of R vector is determined by the ratio of the imaginary and real parts of the susceptibility $\tilde{\eta}_{10}$, i.e., as the R vector approaches the origin (at very large positive or negative values of the deviation angle), the R contour is tangent to the complex susceptibility. Thereby, the orientation of R contour on the complex plane is determined by the initial phase of R vector for electronic and various cases of nuclear scattering.

The R contour a shows the angular evolution of the complex reflection coefficient for electronic scattering. In this case, the susceptibility $\chi_{10}^{\sigma\sigma}$ is mainly the real negative number, so that the initial phase of the reflected wave is close to $-180°$. It remains so while the angle of incidence is not close to the Bragg region. As the Bragg reflection region is approached, the length of the R vector grows and reaches at a certain angle unity. Thus, the amplitude of the reflected wave at the reflecting atomic planes becomes comparable to the amplitude of the incident wave, but the two waves remain in

the opposite phase. This angle corresponds to the left angular border of the region of strong reflection. Further in the region of Bragg reflection, the R vector is rotated clockwise, as it is shown in the left panel of Fig. 2 (contour a), and its phase changes in the angular range of $-180° \rightarrow -360°$. In this region, the length of the vector decreases from unity to zero.

The R contour b displays transformation of the reflection coefficient in the case of nuclear resonant scattering. The incident radiation excites here the nuclear transition $-\frac{1}{2} \rightarrow -\frac{1}{2}$ with the change of the magnetic quantum number $M = 0$. Relative to the case of electronic scattering, the drastic difference in several respects is observed. First of all, the R contour b possesses quite different shape: it looks symmetric relative to the Bragg position. The contour is turned 90° counterclockwise relative to that of electronic scattering because the initial phase of the reflected wave is $-90°$, due to the fact that the susceptibility $\eta_{10}^{\pi\pi}$ is a negative pure imaginary number. At increasing incidence angle, the R vector rotates clockwise, and the phase of the reflected wave changes in the angular range of $-90° \rightarrow -270°$. The length of the R vector changes symmetrically relative to the Bragg angle, and the vector equals unity in the Bragg position. In this position, the amplitude of the reflected wave gets equal to the amplitude of the incident wave, and the waves appear to be in the opposite phases.

The behavior of the R vector in the contour c, which corresponds to resonant scattering for the nuclear transition $-\frac{1}{2} \rightarrow -\frac{3}{2}$, is similar to that considered above. The only difference is in the relative phasing the waves, which changes in the diapason of $-125° \rightarrow -305°$.

The described appearance of the R contours in nuclear scattering is relevant for scattering at the exact resonance. When stepping aside from the resonant energy, the form and the position of the R contours become different. If the energy of incident radiation is shifted by $\mp\Gamma/2$ to the left or to the right slopes of the resonance, the factor $(-i)$ in the susceptibility described by Eq. (7) is replaced by the factors $\pm\frac{1}{2}(1-i)$, which correspond to the rotation of the nuclear R contour by $\pm\pi/4$ angles. In addition to the rotation, the shapes of the contours become asymmetric.

B. Interaction of the wave field with atoms under diffraction conditions

In the case of electronic scattering, we deal with the interaction of the electric component of the wave field with the electric dipole induced in the atomic shell. As for the case of nuclear scattering, the magnetic component of the field interacts with the magnetic dipole of the excited transition in ^{57}Fe nucleus. The amplitude of the magnetic wave field is determined, as well as the amplitude of the electric wave field, by Eq. (1), where the scalar amplitudes E must be replaced by the amplitudes H and the polarization vectors $\mathbf{e}$ by the polarization vectors $\mathbf{h}$. In the cases of the contours a and b, the σ- and π-polarized waves are incident on the crystal with the relations $\mathbf{e}_1^\sigma = \mathbf{e}_0^\sigma$ and $\mathbf{h}_1^\pi = \mathbf{h}_0^\pi$, respectively (see Fig. 1). Because the polarization vectors of the incident and the reflected waves are the same, the E_{tot} and H_{tot} contours of the total wave amplitudes at the reflecting atomic planes are

easily obtained, simply by shifting the axis of the imaginary values to the left-hand side by unity (see the upper panel in Fig. 2). The new axes are $\text{Re}(1+R)$ and $\text{Im}(1+R)$. The total field amplitudes far away from the Bragg angle are $E_{\text{tot}} = E_0$ and $H_{\text{tot}} = H_0$ (E_0 and H_0 are assumed to be equal to unity). The length of the E_{tot} vector decreases from unity to zero keeping its orientation, then it starts to grow rotating at the same time clockwise. The H_{tot} vector starts rotating clockwise immediately, and its length decreases from unity to zero at the first stage. While reaching the Bragg angle, the total field H_{tot} disappears and then grows symmetrically up to the value of $H_0 = 1$. The angular dependencies of the absolute values of the field amplitudes E_{tot} and H_{tot} at an arbitrary reflecting plane for electronic and nuclear scatterings are shown in the lower panel of Fig. 2. When approaching the Bragg region, the strength of the electromagnetic field at the atomic planes drops down in any of the considered cases. At a definite angular position, the field at atoms completely disappears in both electronic and nuclear scattering. But, as the angle increases further, the behavior of the fields becomes strongly different. For nuclear scattering, the amplitude of the field H_{tot} symmetrically increases, approaching gradually the level of the incident wave amplitude. In electronic scattering, however, the field amplitude E_{tot} first sharply rises to the value significantly exceeding the amplitude of the incident wave, and then falls down to this level. The extraordinary rise of the total electric wave field is determined by the constructive interference of the propagating and the reflected waves when moving along the R contour, as one can see in the left panel of Fig. 2. The dramatic transformation of E_{tot} occurs within rather narrow angular range, while H_{tot} dependence spreads over much broader region. The characteristic angular ranges are determined by the magnitudes of electronic and nuclear susceptibilities.

The diminishing of the total field amplitudes at the atomic planes to zero corresponds to the Borrmann effect for electronic scattering [13] and to the Kagan-Afanas'ev effect for nuclear scattering [11]. In the first case, the absorption of x rays by electrons gets negligibly small [14], while in the second case the inelastic channels of nuclear reaction are getting completely suppressed [11,15]. For the considered examples, the polarization vectors of the incident and reflected waves are collinear. This is the decisive condition for turning down the total field at the atoms and for the decrease of the x-ray absorption by atoms. However, whereas for realization of the Borrmann effect the disappearance of the fields at the atoms is a necessary condition, for the Kagan-Afanasev effect it is optional, as we shall see below.

We consider a situation, where the polarization vectors of the incident and the reflected waves are not collinear: $\mathbf{e}_1^\pi \neq \mathbf{e}_0^\pi$ and $\mathbf{h}_1^\sigma \neq \mathbf{h}_0^\sigma$ (see Fig. 1). In these cases, at the Bragg angle we obtain, using Eq. (1) and Table II, the following relations: $\mathbf{E}_{\text{tot}}(\mathbf{r}_m) \propto E_0[\mathbf{e}_0^\pi - \mathbf{e}_1^\pi]$ and $\mathbf{H}_{\text{tot}}(\mathbf{r}_m) \propto H_0[\mathbf{h}_0^\sigma - \mathbf{h}_1^\sigma \exp(-i2\theta)]$. In both cases, the amplitudes of the incident and reflected waves are equal in absolute values, but the amplitude of the total field at the atoms of the reflecting planes turns out to be a finite value. Consequently, the condition for the Borrmann effect is violated and, therefore, the strong residual absorption of radiation by an electron shell takes place.
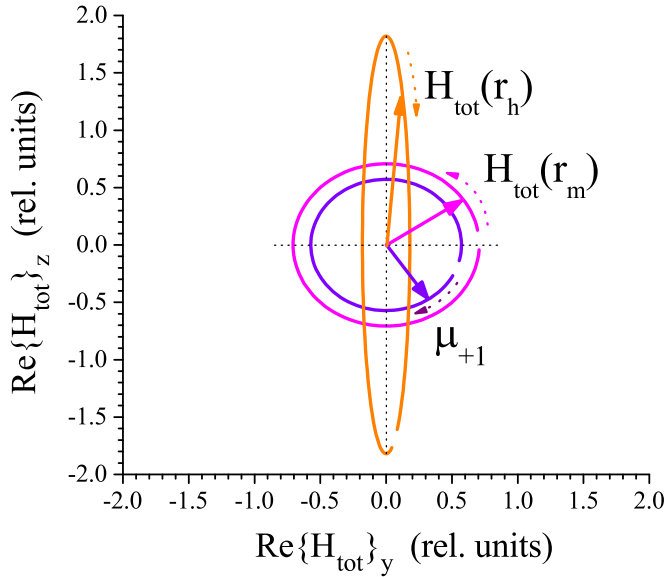
FIG. 3. The time trajectories of the end points for the field strength vector: $\mathbf{H}_{tot}(\mathbf{r}_m, t)$ at the reflecting atomic planes, $\mathbf{H}_{tot}(\mathbf{r}_h, t)$ at the middle plane between the reflecting planes, and of the excited magnetic moment vector μ_{+1} for the nuclear transition $-\frac{1}{2} \to -\frac{3}{2}$.

Now, we consider the scenario for nuclear scattering. We write the expression for the total field, taking into account the temporal dependence of its amplitude:

$$\mathbf{H}_{tot}(\mathbf{r}_m, t) \propto \exp{(i\omega t)}H_0\big[\mathbf{h}_0^\sigma - \mathbf{h}_1^\sigma \exp{(-i2\theta)}\big]. \quad (8)$$

In order to analyze the time dependence of the complex vector $\mathbf{H}_{tot}(\mathbf{r}_m, t)$, we evaluate the real part of the expression presented above: $\text{Re}[\mathbf{H}_{tot}(\mathbf{r}_m, t)] = \mathbf{h}_0^\sigma \cos\omega t - \mathbf{h}_1^\sigma \cos 2\theta \cos\omega t - \mathbf{h}_1^\sigma \sin 2\theta \sin\omega t$. For the determined real vector, we calculate its projections on the Y and Z axes [taking into account that $h_{0y}^\sigma = \sin\theta$, $h_{0z}^\sigma = -\cos\theta$ and $h_{1y}^\sigma = -\sin\theta$, $h_{1z}^\sigma = -\cos\theta$ (see Fig. 1)], obtaining $\text{Re}[\mathbf{H}_{tot}(\mathbf{r}_m, t)]_Y = \sin\theta \cos\omega t + \sin\theta \cos 2\theta \cos\omega t + \sin\theta \sin 2\theta \sin\omega t$ and $\text{Re}[\mathbf{H}_{tot}(\mathbf{r}_m, t)]_Z = -\cos\theta \cos\omega t + \cos\theta \cos 2\theta \cos\omega t + \cos\theta \sin 2\theta \sin\omega t$. At last, the time dependence of the total field strength can be presented on the complex plane with the axes $\text{Re}[\mathbf{H}_{tot}]_Y$, $\text{Re}[\mathbf{H}_{tot}]_Z$ as follows:

$$H_{tot}(\mathbf{r}_m, t) = \sin 2\theta \exp{[i(\omega t - \theta)]}. \quad (9)$$

The obtained expression represents the left-handed circularly polarized field. The counterclockwise circulation of the magnetic field strength vector within a time period is shown in Fig. 3. The field amplitude $|\mathbf{H}_{tot}| = \sin 2\theta$ amounts to a significant part of the incident wave amplitude, $\sim 0.57 H_0$, the initial phase of H_{tot} is $-\theta$.

The question is whether the field of such a form is able to excite the nuclear transition $-\frac{1}{2} \to -\frac{3}{2}$. The orientation of the magnetic moment in space is determined by the following unit vector:

$$\mu \propto \mathbf{n}_{-M}, \quad M = m_e - m_g, \quad \mathbf{n}_{-M} = \mathbf{n}_{+1},$$

where the unit vector $\mathbf{n}_{+1} = -(\mathbf{n}_y + i\mathbf{n}_z)/\sqrt{2}$. This gives the following expression for the temporal behavior of the magnetic moment: $\mu_{+1}(t) \propto \exp{(i\omega t)}(\mathbf{n}_y + i\mathbf{n}_z)$. Then, the real part of $\mu_{+1}(t)$ is $\text{Re}\{\exp{(i\omega t)}(\mathbf{n}_y + i\mathbf{n}_z)\} = (\mathbf{n}_y \cos\omega t - \mathbf{n}_z \sin\omega t)$, and the projections of the obtained vector on Y, Z axes are $\text{Re}\{\exp{(\omega t)}(\mathbf{n}_y + i\mathbf{n}_z)\}_Y \propto \cos\omega t$ and $\text{Re}\{\exp{(\omega t)}(\mathbf{n}_y + i\mathbf{n}_z)\}_Z \propto -\sin\omega t$. The result of the calculation shows that the vector rotates clockwise, that is in the direction opposite to the rotation of the vector $\mathbf{H}_{tot}$ (see Fig. 3). Therefore, when the frequency of the primary radiation is tuned to excite the given nuclear transition, the total field created by the nuclear ensemble at the Bragg angle is not able to produce the excitation of nuclei because of the opposite directions of the circular polarizations of the field and of the relevant magnetic moment. This result demonstrates the unique property of the Kagan-Afanas'ev effect, the effect of suppression of inelastic channels of nuclear reaction. In contrast to the Borrmann effect, where the necessary condition is the cancellation of the amplitude of the electromagnetic field at the atoms, the requirement for an observation of the Kagan-Afanas'ev effect turns out to be *the suppression of the amplitude of nuclear excitation*. As we have seen, this condition can be fulfilled even if the field amplitude at the atoms is quite large.

We turn to consider the question as to how the wave field configuration in space between the neighboring reflecting atomic planes is modified due to diffraction. As mentioned in Sec. II A, the field amplitude is modulated in the direction orthogonal to the scattering planes. When the angle of incidence approaches the Bragg angle, a standing wave is formed. For nuclear scattering, the structure of the standing wave can be completely different for different nuclear transitions.

As we have seen, in nuclear scattering for the transition $-\frac{1}{2} \to -\frac{1}{2}$, where $M = 0$, the standing wave is built up with the magnetic field nodes located in the reflecting planes, at $\mathbf{r} = \mathbf{r}_m$. In the plane lying in the middle between the reflecting planes, the phase factor $\exp{(i\mathbf{S}\mathbf{r}_h)} = -1$. Therefore, in these planes the magnetic components of the incident and reflected electromagnetic waves add constructively, forming antinodes of the magnetic field. There, the magnetic field amplitude is $|\mathbf{H}_{tot}| = 2H_0$, and the field is linearly π polarized.

In contrast, the amplitude of the magnetic component of the wave field at the reflecting planes for nuclear scattering with the transition $-\frac{1}{2} \to -\frac{3}{2}$ is finite. In this case, the wave is left-hand circularly polarized and, as shown above, with such a polarization, it is not capable to excite nuclei. Concerning the field in the middle plane, it is given by the following expression:

$$\mathbf{H}_{tot}(\mathbf{r}_h, t) \propto \exp{(i\omega t)}H_0\big[\mathbf{h}_0^\sigma + \mathbf{h}_1^\sigma \exp{(-i2\theta)}\big] \quad (10)$$

[compare to Eq. (8)]. The right-handed circulation of the field vector at the middle plane within a time period is displayed in Fig. 3. Evidently, the field is elliptically polarized. The ellipse is strongly extended along the Z axis, i.e., in the direction of the σ-polarization vector. We see that the polarization state of the standing wave underwent a dramatic transformation in the space interval between the reflecting plane and the middle plane. The presented example vividly demonstrates one more peculiar feature of nuclear diffraction.

Electronic scattering linear σ polarization

Nuclear scattering M=0 transition linear π polarization

Nuclear scattering M=−1 transition elliptic polarization
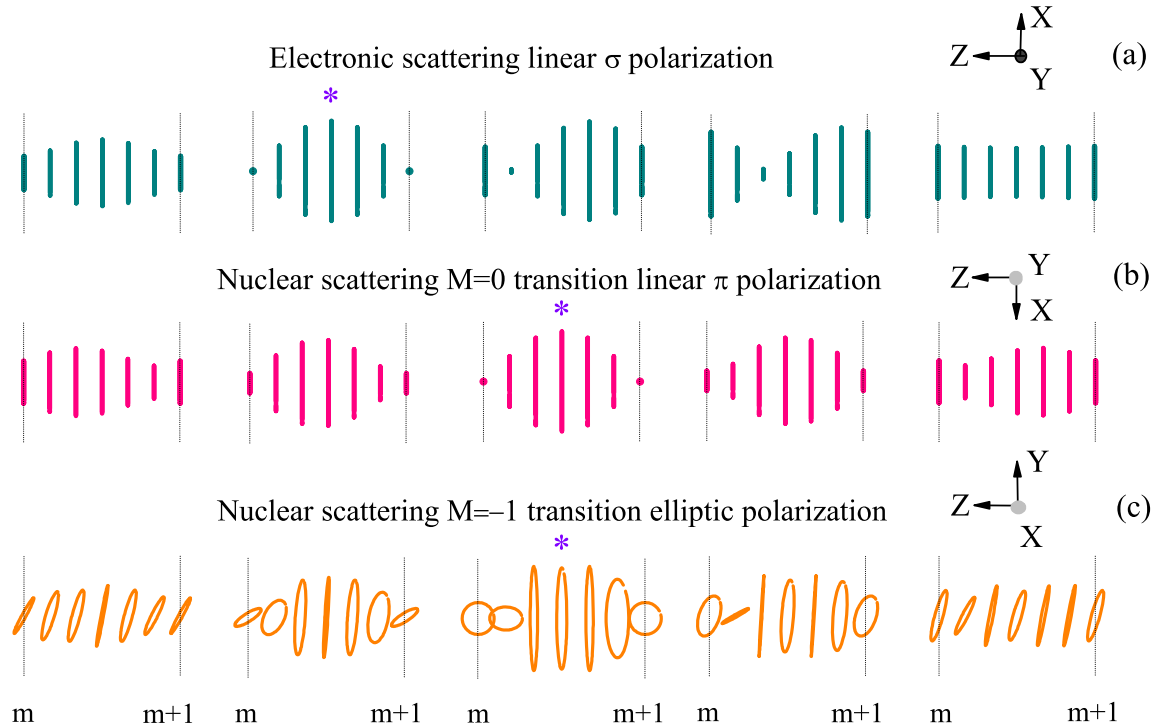
FIG. 4. Structure of the modulated wave field in the space between the reflecting atomic planes m and $m + 1$ for several angular positions of the crystal in the vicinity of the Bragg angle. The set of panels (a) illustrates the case of electronic scattering, the sets of panels (b) and (c) are related to the case of nuclear resonant scattering. The angle of incidence of radiation is increased from panel to panel from the left-hand to the right-hand side, corresponding to the angular deviations of $-260, -25, 0, +25,$ and $+260$ μrad from the center of the rocking curve. The angular positions corresponding to the left edge of the range of the strong electronic reflection and to the angle of maximum nuclear reflection are marked by the stars. The bold vertical bars on the panels (a) and (b) and the ellipses in the set of panels (c) display linear and elliptical oscillations of the electric strength vectors for electronic scattering and of the magnetic strength vectors for nuclear scattering in the equally spaced points between the reflecting planes. In nuclear scattering, the transitions $-\frac{1}{2} \rightarrow -\frac{1}{2}$ (b) and $-\frac{1}{2} \rightarrow -\frac{3}{2}$ (c) are excited, respectively. All oscillations are displayed in the XYZ coordinate system.

C. Standing wave structure

In the case of electronic scattering, various questions concerning the wave field spatial distribution in crystals have been investigated in details [16,17]. Concerning nuclear scattering, the examples of transformation of the electromagnetic field polarization within one unit cell under conditions of realization of the effect of suppression of nuclear excitation are presented in Ref. [18]. The expressions for the wave field amplitude at the atomic planes and between them in the approximation of small deviations from the Bragg angle are given in Ref. [9], Eqs. (5) and (6). Different behavior of the field in the cases of electronic and nuclear scattering for the transition with $\Delta M = 0$ is illustrated in Ref. [9], in Fig. 5. In this work, spatial distributions of the wave field oscillations are found for arbitrary angles of incidence in the range of Bragg reflection. For each angle, the distributions along the normal to the reflecting planes are calculated in the space interval between the atomic planes m and $m + 1$. The results of the calculations for electronic scattering and nuclear scattering for the transitions $-\frac{1}{2} \rightarrow -\frac{1}{2}$ and $-\frac{1}{2} \rightarrow -\frac{3}{2}$ are presented in Fig. 4. The scattering geometry is symmetric.

Figure 4(a) displays evolution of the amplitude modulation and the spatial location of the total electric wave field in electronic scattering of σ-polarized wave. In this case, the wave field is linear polarized in a way that the oscillations of the electric strength vector occur along X axis, within the limits

of the vertical bold bars in Fig. 4. The amplitude modulation at the initial crystal position is displayed on the left panel. In this angular position ($\theta - \theta_B = 0$ μrad), the electric field amplitude is only slightly different in the atomic planes and between them. The highest contrast is achieved on the left edge of the reflection region, marked by the star, at the angle $\theta - \theta_B = 10.5$ μrad. Herein, the *standing wave* is formed. The nodes of the wave are located at the atomic planes, whereas the antinodes with the doubled amplitude at the middle plane. Thus, the electric field is as if it is completely pushed out to the space unoccupied by atoms. For this reason, the absorption of radiation drops down dramatically. Further on, the wave field is moving along the normal to the reflecting planes, oppositely to the Z-axis direction, practically without changing its configuration, i.e., keeping the shape of the standing wave (the next two distributions correspond to the angles $\theta - \theta_B = 17.5$ and 35 μrad, respectively). Thereby, since the field strength at the atomic planes grows, the absorption of radiation by atoms restores. Nevertheless, the integrated over the sample absorption still plays a negligible role. This happens because, due to *an interference phenomenon, known as primary extinction*, the field is not allowed to penetrate into the crystal within the range of strong reflection (the issues of the primary extinction and of the penetration length will be discussed in Sec. IV C). Drifting further with the increase of the incidence angle, the antinodes of the standing
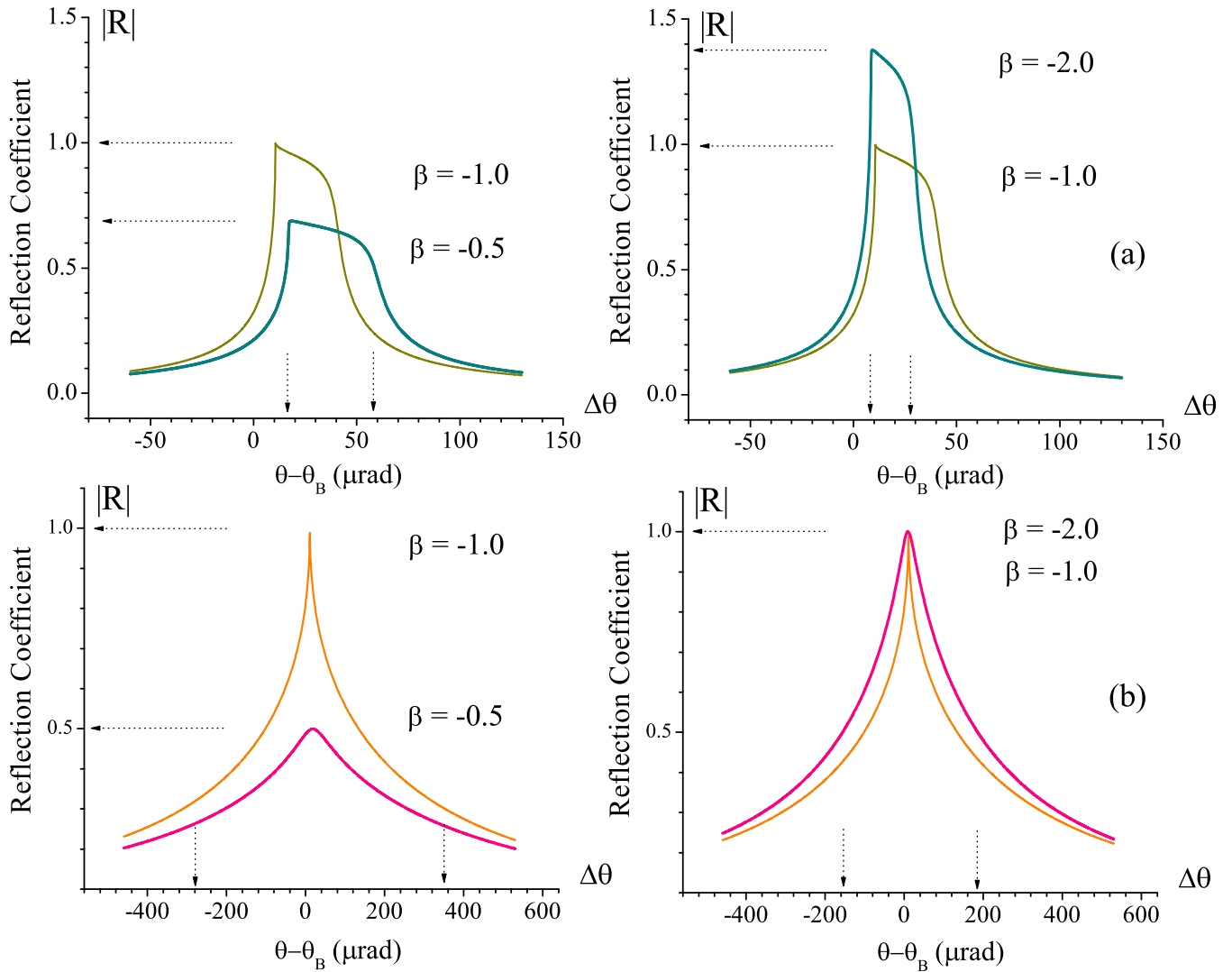
FIG. 5. The angular dependencies of the absolute values of the reflection coefficient: (a) in potential electronic scattering and (b) in resonant scattering with the nuclear transition $-\frac{1}{2} \rightarrow -\frac{1}{2}$. The bold lines depict the dependencies for the asymmetric geometry with $\beta = -0.5$ (left panels) and $\beta = -2.0$ (right panels). For comparison, the dependencies for the symmetric geometry are shown by thin lines. The vertical arrows mark the boundaries of the region of strong reflection in the cases of asymmetric scattering.

wave move to the atomic planes. Because at these angles the primary extinction plays already lesser role, the radiation can penetrate deeper into the crystal and, therefore, the role of absorption increases significantly. Finally, far away from the Bragg region ($\theta - \theta_B = 260 \mu$rad), the reflected wave fades out and only the wave propagating in the forward direction with a constant in space amplitude remains.

Figure 4(b) displays evolution of the spatial modulation of the magnetic wave field amplitude for nuclear resonant scattering of π-polarized incident wave when the nuclear transition $-\frac{1}{2} \rightarrow -\frac{1}{2}$ is excited (scattering by electrons is neglected in these calculations). When the crystal is set in the Bragg position (marked by the star), the standing magnetic wave with the nodes at the atomic planes and the antinodes between the planes is formed. The field is linearly π polarized, oscillations of the magnetic strength vectors occur along the X axis. In this angular position, the field is not absorbed by nuclei, and radiation is able to penetrate deeply into the crystal. When turning the crystal away from the center of

the rocking curve, both to the left-hand and to the right-hand sides by 25 μrad, 260 μrad symmetrically, the modulation of the field amplitude in space decreases. The oscillations of the magnetic field at the atomic planes restore and, therefore, the absorption of radiation by the nuclei appears. It is interesting to note that, in contrast to the case of electronic scattering, the modulation pattern only slightly shifts along the normal to the reflecting planes when the crystal angular setting changes. In addition, the offset direction depends on the direction of rotation of the crystal.

The evolution of the total magnetic field spatial distribution in nuclear resonant scattering of σ-polarized wave is shown in in Fig. 4(c). When the crystal is magnetized along the X axis, the incident radiation can excite only the nuclear transitions with $\Delta M = \pm 1$, in the particular case, the transition $-\frac{1}{2} \rightarrow -\frac{3}{2}$. In this case, one observes quite a different picture: now the total field of the elliptical polarization is created. The rotation of the magnetic strength vector occurs in the YZ plane. The pure circular rotation of the magnetic vector takes

place in the atomic planes when the crystal is set at the Bragg position (marked by the star). Yet, as we were convinced above, the left circular polarized field is unable to excite the right circular polarized oscillation of the nuclear transition magnetic moment. Therefore, in the absence of absorption the field is capable to penetrate deeply into the crystal. To the left- and to the right-hand sides from the Bragg position, the field at the atomic planes becomes elliptically polarized. Therefore, the absorption of radiation by nuclei is partly restored. The noticeable asymmetry of the field configurations at the opposite sides of the Bragg angle is observed. In the limit of the large angular deviation, only the σ-polarized wave propagating through the crystal remains. In general, the fanciful patterns of the transforming polarization are observed in the considered case.

D. Interplay between absorption and reflectivity

We recall that the reflectivity of a crystal is defined by the expression $Q = |R|^2/|\beta|$ [see Eq. (5)]. When the scattering geometry is symmetric, it represents the ratio of intensities in the diffracted and the incident beams. In this case, for nuclear resonant diffraction the full reflectivity $Q = |R|^2$ approaches unity [see the angular behavior of the reflection coefficient in Figs. 2 and 5(b)]. The prediction of the 100% reflectivity of γ radiation by nuclear lattice [8] was very unexpected. Indeed, high reflectivity looks improbable if one takes into account that the intermediate state only to a small percentage decays by reemission of γ radiation. Most of the radiation should be lost into incoherent decay channels via internal conversion and spin-flip processes. Furthermore, losses can be expected from the diffraction process itself, which gives rise to incoherent channels due to an isotopic and spin incoherence. In the case of ^{57}Fe, the entire losses into incoherent channels should amount to at least 95%. Under these circumstances, it was hard to imagine that in the resonance Bragg diffraction of γ rays high reflectivity might be ever reached.

The main reason of the high reflectivity turned out to be the suppression of all inelastic channels of nuclear scattering, Kagan-Afanas'ev effect, discussed in Sec. III B. The nature of the suppression is related to the formation of the interference pattern described in Sec. III C. Due to the formation of the standing wave field inside the crystal, the amplitude of nuclear excitation can be strongly modified. In particular, when the field nodes are formed at the place of nuclear positions, the excitation of nuclei vanishes.

Clearly, in this situation we face an obvious logical confusion: the total reflection of γ radiation is only possible because of the full suppression of nuclear absorption. The latter is caused by forcing the excitation amplitude to zero. One should then conclude that *the entire reflection takes place under conditions where the excitation amplitude becomes zero*, which sounds really puzzling. This question can be answered if we closely consider the interaction of the total wave field with nuclei, namely, the issues of the interplay of absorption and diffraction of radiation near the Bragg position [19].

The damping of the field intensity inside a semi-infinite crystal is given by the linear absorption coefficient $\mu_a = 2K \,\mathrm{Im}\varepsilon_0^{(2)}$, i.e., by the imaginary part of $\varepsilon_0^{(2)}$ [see Eq. (1)]. At resonance, where $\eta_{dd'} = i\eta$, and for the symmetric case

$\beta = -1$, the expression for $\varepsilon_0^{(1,2)}$, Eq. (2) takes the simple form

$$\varepsilon_0^{(1,2)} = \tfrac{1}{4}\{\alpha \mp \sqrt{\alpha^2 - 4i\eta\alpha}\}. \tag{11}$$

From Eq. (11), it can be immediately deduced that $\mathrm{Im}\varepsilon_0^{(2)}$ falls down from $\frac{1}{2}\eta$ to zero when approaching Bragg position. This means that in the entire angular range around the Bragg position, the damping is less than the off-Bragg regular damping caused by the absorption in resonance. Thus, in resonance diffraction there is no anomalously strong damping similar to the primary extinction characteristic for electronic Bragg scattering of x rays. On the contrary, the radiation is allowed to penetrate into the crystal deeper than it does in the off-Bragg position of the crystal.

The weakest damping and the deepest penetration obviously occur when the exact Bragg position is reached. In the immediate neighborhood of the Bragg position where $\alpha \ll \eta$, we may approximately accept that $\varepsilon_0^{(1,2)} \sim \frac{1}{4}\{\alpha \pm \sqrt{2\alpha\eta}(1-i)\}$ and, hence, $\mathrm{Im}\varepsilon_0^{(2)} \sim \sqrt{\alpha}$. The total number N of nuclei interacting with the field is proportional to the penetration length L_a of radiation. Because $|\mu_a L_a| = 1$, the penetration length is inversely proportional to $\mathrm{Im}\varepsilon_0^{(2)}$, which yields the angular dependence $N \sim 1/\sqrt{\alpha}$.

For the radiation polarization component with $\mathbf{h}_1 = \mathbf{h}_0$, the wave field amplitude at the reflecting planes, where $\exp(i\mathbf{S}\mathbf{r}_m) = 1$, is given by

$$\mathbf{H}(\mathbf{r_m}) \sim \exp\left(\tfrac{1}{4}K\sqrt{\alpha\eta}L\right)\left\{1 + \frac{i\eta}{\tfrac{1}{2}[\alpha + (1-i)\sqrt{\alpha\eta}] - i\eta}\right\}\mathbf{h}_0. \tag{12}$$

In the approximation of $\sqrt{\alpha} \ll \sqrt{\eta}$, it is proportional to

$$\mathbf{H}(\mathbf{r}_m) \sim \exp\left(-\tfrac{1}{4}\sqrt{\alpha\eta}KL\right)\sqrt{\frac{\alpha}{\eta}}. \tag{13}$$

The question now concerns the entire absorption and reflection of the wave field over the increased penetration length. Both the entire absorption and reflection are determined by the total number of nuclei $N \sim 1/\sqrt{\alpha}$, and by the field amplitude at the positions of nuclei $\mathbf{H}(\mathbf{r}_m) \sim \sqrt{\alpha}$. We recall that α is the deviation from the Bragg angle. Lowering of the field amplitude is accompanied by growing with the same tempo of the number of reflecting nuclei.

When absorption is considered, the contributions of all nuclei are summed incoherently. The entire absorption then turns out to be given by

$$\text{entire absorption } \sim N \times |\mathbf{H}(\mathbf{r}_m)|^2 \sim (1/\sqrt{\alpha})\alpha = \sqrt{\alpha} \tag{14}$$

and, hence, diminishes proportionally to $\sqrt{\alpha}$. At the exact Bragg position, the entire absorption completely vanishes. This results in a suppression of incoherent channels. But, when diffraction is considered, the contributions of all nuclei should be summed coherently. The reflection is then given by the square of the summary scattering amplitude

$$\text{reflection } \sim |N \times \mathbf{H}(\mathbf{r}_m)|^2 \sim |(1/\sqrt{\alpha})\sqrt{\alpha}| = 1. \tag{15}$$

In spite of the vanishing wave field when approaching the Bragg position, reflection does not vanish. In contrast, at the Bragg position it becomes the total one. Thus, we see

that the coherent scattering of all nuclei is able to maintain diffraction, even though the field amplitude at the place of each individual nucleus vanishes. The different behavior of the total absorption and total diffraction is of course due to the different ways of summing the contributions of all the nuclei.

Thus, in resonance Bragg diffraction, in spite of the very strong incoherent channels for individual nuclei, diffraction can take place without absorption. In a semi-infinite crystal, the only outlet for the radiation is the entrance surface. The entire radiation must leave the crystal through this surface; this is the reason why the total reflection is achieved in spite of the very deep penetration.

IV. ROLE OF THE ASYMMETRY OF THE DIFFRACTION GEOMETRY

A. Absolute value of the reflection coefficient

In Fig. 5, the angular dependencies of the absolute values of the reflection coefficient $|R|$ are presented for the asymmetric geometries with the asymmetry factors $\beta = -0.5$ and -2.0.

First, we consider an event of potential scattering of radiation by electrons [see Fig. 5(a)]. In this case, there is a pronounced angular range, where the reflection coefficient is maximal and changes slightly. The boundaries of this range are marked by the vertical arrows. Let us find the width and the center position of this range. Here, we should consider only the electron susceptibility, so that $\tilde{\eta}_{dd'} = \chi_{dd'}$. Given that $|\mathrm{Im}\chi_{dd'}/\mathrm{Re}\chi_{dd'}| \ll 1$, one can approximately write the root in the expression for ε in the form $\sqrt{[\chi'_{00} + \chi'_{11}|\beta| - \alpha|\beta|]^2 - 4|\beta|(\chi'_{01}\chi'_{10})}$, where the prime symbol designates the real value of the susceptibility. The solution has a physical sense only if the expression under the square root is greater than or equal to zero. This condition yields the formulas for the left and right boundaries of the strong reflection region as $\alpha_{1,2} \approx \chi'_{00}/|\beta| + \chi'_{11} \pm 2\sqrt{(\chi'_{01}\chi'_{10})}/\sqrt{|\beta|}$, wherein one gets the expressions for the center position and for the width of the strong reflection range as

$$\alpha_c = \chi'_{00}/|\beta| + \chi'_{11},$$
$$|\Delta\alpha| = 4\sqrt{(\chi'_{01}\chi'_{10})/|\beta|}. \qquad (16)$$

As one can see from Eq. (16), at rising $|\beta|$ the angular width of the range decreases in inverse proportion to $\sqrt{|\beta|}$. Substituting the susceptibility values given in Table II and taking into account the relation between the angular parameter α and the real angle, we obtain $|\Delta\theta| = (59.2 - 17.1) = 42.1 \ \mu$ rad for $|\beta| = 0.5$ and $|\Delta\theta| = (29.6 - 8.5) = 21.1 \ \mu$rad for $|\beta| = 2.0$, which is in agreement with the data in Fig. 5(a). With the increase of $|\beta|$, the center position of the reflection range approaches the value of χ'_{11}. Remarkably, the shrinking of the reflection range is accompanied by the growth of the maximal magnitude of the reflection coefficient $|R|_m$. Notice that $|R|_m$ is less than unity for $|\beta| < 1$ and more than unity for $|\beta| > 1$. Thus, in the case of a constructive interference, where $\exp(i\mathbf{Sr}_m) = 1$, the amplitude of the reflected wave at the reflecting plane appears to be in the first case lesser, while in the second case larger than the amplitude of the wave incident

on the reflecting plane. It is easy to show that for $|\beta| > 1$ and the angular parameter $\alpha_m \approx \alpha_c \to \chi'_{11}$, the maximal value of the reflection coefficient obeys the dependence

$$|R|_m \approx \left| \frac{\beta q}{\frac{1}{2} + \sqrt{1 - 4|\beta||q^2}} \right|, \qquad (17)$$

where $q = (\chi'_{01}/\chi'_{00})$. The dependencies of the maximal value of the reflection coefficient $|R|_m$ and of the width of the reflection range $|R|_w = \Delta\alpha$ in the case of potential electronic scattering are presented on left-hand panel in Fig. 6. As one can see, when moving from the range of the grazing to the range of the steep incidence of x rays, the absolute value of the reflection coefficient monotonously grows, and the reflection diapason narrows. At upper extreme of this range, the amplitude of the reflected wave can exceed that of the incident wave by more than five times.

We turn to the case of nuclear resonant scattering. Here, the behavior of the reflection coefficient has a number of significant differences. The shape of the angular dependence of the absolute value of the reflection coefficient resembles a symmetrical peak, as one can see in Fig. 5(b). Thus, in contrast to the case of electronic scattering, the clear-cut range of a strong scattering is absent. One can expect similar properties of angular dependence of Bragg scattering in neutron resonant scattering [20] and at an absorption edge in x-ray scattering in the case of the large imaginary part relative to the real part of scattering amplitude, as discussed in Ref. [19] (see Fig. 5 in that paper). At the same time, the widths of the angular dependencies exceed those in the case of electronic scattering by more than an order of magnitude. As discussed above, this difference is determined by the ratio of the nuclear and the electronic susceptibilities $|\eta|/|\chi|$, which essentially exceeds unity (see Table II). The maximal absolute value of the reflection coefficient and the angular width of the relevant curve at the half-height as functions of the asymmetry factor in resonance Bragg diffraction are shown on the right-hand panel in Fig. 6. Here, in contrast to the case of potential electronic scattering, the width of the angular curve grows when moving apart from the symmetric geometry, both to the side of the grazing incidence geometry ($|\beta| < 1$) and to the side of the steep incidence geometry ($|\beta| > 1$). However, when moving toward large $|\beta|$, the rise of the angular curve width slows down. As far as the maximal absolute value of the reflection coefficient is concerned, it grows within the entire range of increasing $|\beta|$, with the very fast increase in the range of $|\beta| < 1$. The rise abruptly slows down in the interval of $1 < |\beta| < 2$, and practically ceases at $|\beta| > 2$. The absolute value of the reflection coefficient does not exceed unity in contrast to the case of electronic scattering.

As to the reflectivity, its maximum value $Q \sim 1$ in electronic scattering is reached at any magnitude of the asymmetry factor with the only difference that in the grazing incidence geometry $|\beta| < 1$, it occurs in a broader angular range, while in the steep incidence geometry $|\beta| > 1$, it happens in a narrower range (see Fig. 7, left panel). In nuclear scattering, the maximum reflectivity $Q \sim 1$ is reached only for the symmetric diffraction geometry (Fig. 7, right panel). When stepping aside from the point of symmetry toward either direction, the nuclear reflectivity drops down. The reflectivity
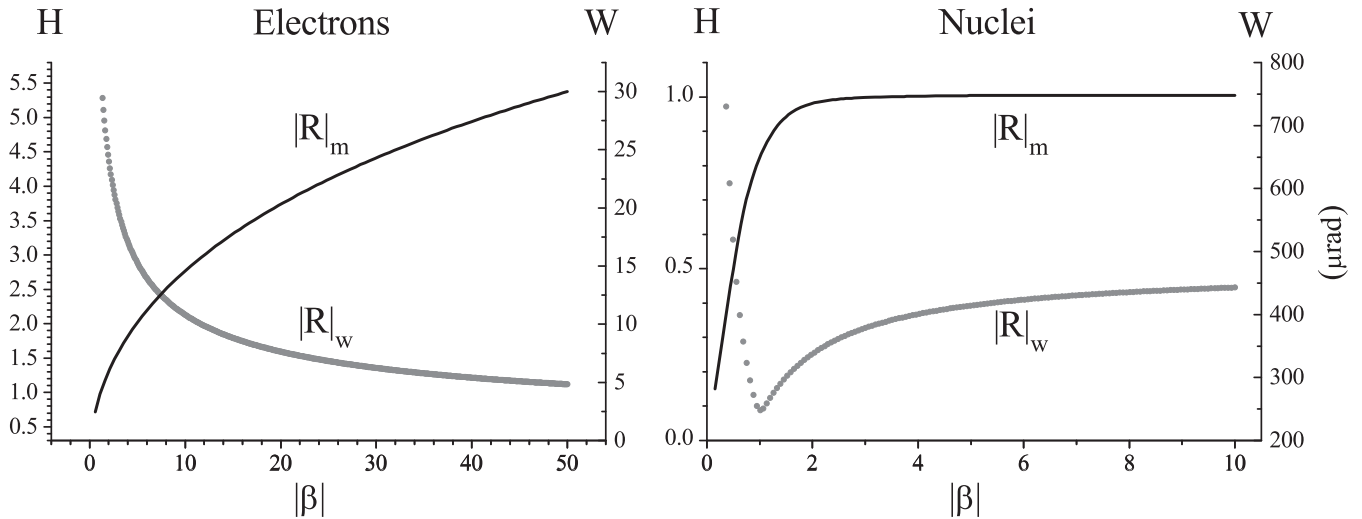
FIG. 6. The maximal value of the reflection coefficient $|R|_m$ (shown by the vertical left-hand axis H) and of the width of the reflection range $|R|_w$ (shown by the vertical right-hand axis W) as a function of the asymmetry factor $|\beta|$, with the left-hand panel for the case of electronic scattering and the right-hand panel for the case of nuclear scattering with the transition $\frac{1}{2} \rightarrow -\frac{1}{2}$.

of about half the maximum value is reached for the considered cases of asymmetry.

B. Transformation of the total wave field when passing toward asymmetric geometry

Figure 8 shows the distributions of the wave field amplitudes in the space between the neighboring atomic planes for various scattering geometries and, in each geometry, for several incidence angles. In the center panels, the spatial distribution is given for the symmetric geometry $\beta = -1$. In the left- and the right-hand panels, they are shown for the asymmetric geometry in the grazing incidence case with $\beta = -0.5$, and in the steep incidence case with $\beta = -2.0$, respectively. The amplitude of the wave propagating in the direction of $\mathbf{k}_0$ vector is taken for unity.

First, we consider the upper row of the panels illustrating the case of electronic scattering. The spatial distributions of the electric field amplitude $|\mathbf{E}_{\text{tot}}|$ are shown here. The distribution in the symmetric geometry is related to that in Fig. 4(a). When approaching the Bragg range, the reflected wave starts to be formed, and a slight modulation of the wave field amplitude appears, as shown by the thickest orange line. At the left edge of the reflecting range, a maximum contrast of modulation is reached (as shown by the thinner green line). The electromagnetic field is completely pushed out into the space between the planes. With a further increase of the angle, the maximum of the wave field amplitude moves toward the atomic planes (shown by the further thinner pink line). When getting out of the reflection range, the modulation contrast gradually drops down (the consequently thinner violet and blue lines). Here, the modulation of the amplitude turns out
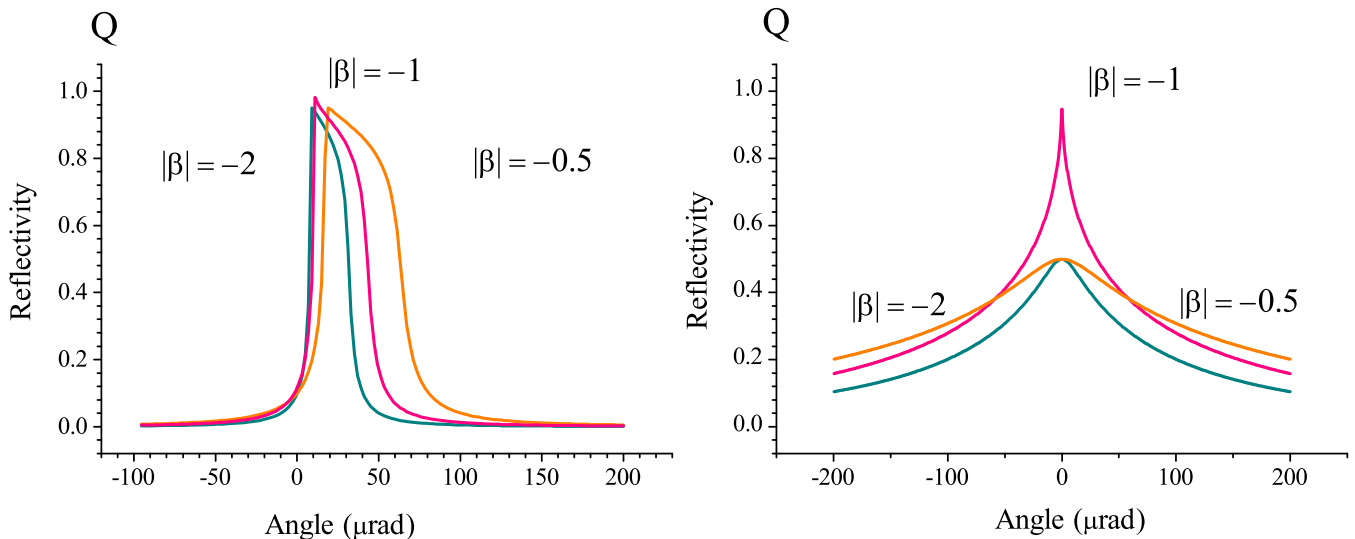
FIG. 7. The angular dependence of the reflectivity in the case of electronic (left panel) and nuclear scattering for $M = 0$ transition (right panel) for three indicated values of the asymmetry factor.
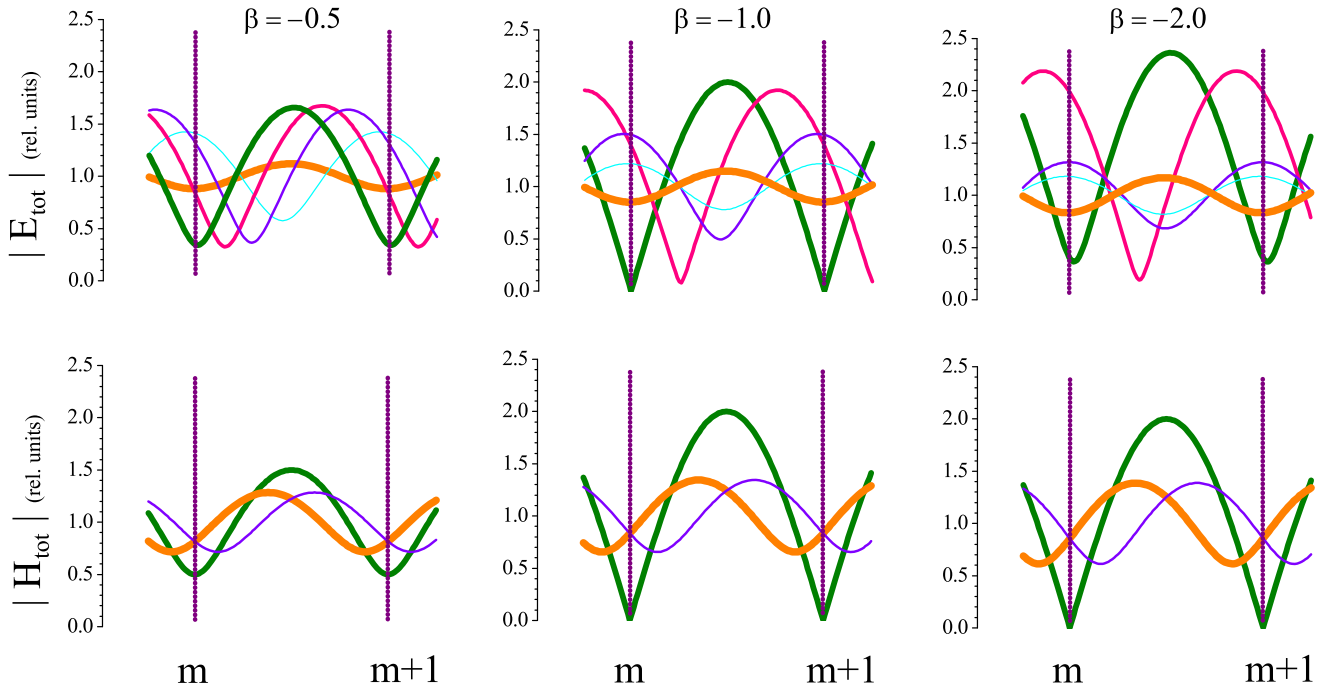
FIG. 8. The distributions of the wave field amplitude in the space between the neighboring atomic planes m and $m + 1$ at various angles of incidence of radiation on the crystal in the vicinity of the Bragg angle, shown for various magnitudes of the asymmetry factor β. The upper row of panels correspond to scattering of σ-polarized wave by electron shells of atoms; the lower row correspond to scattering of π-polarized wave by atomic nuclei when the nuclear transition $-\frac{1}{2} \rightarrow -\frac{1}{2}$ is excited. The amplitude of the wave incident on the planes is taken equal to unity. The thickest orange lines correspond to angles lesser than the Bragg angle, the thinner green lines correspond to angles on the left edges of the range of strong reflection for electronic scattering and to the Bragg angle for nuclear scattering. The subsequently further thinner pink, violet, and blue lines correspond to sequentially increasing angles above the Bragg angle.

to be inverted relative to that at the entrance of the reflection range, e.g., compare the thicker orange and blue lines.

The picture does not change qualitatively in the asymmetric geometry. However, here there are quantitative differences. The main difference is in the modulation contrast. At the grazing incidence (as shown by left-hand panel), the contrast of modulation is much less than in the symmetric case. The wave field amplitude at the atomic planes is not zero for all incidence angles. At the steep incidence (see right-hand panel), the modulation contrast, on the contrary, is getting larger than in the symmetric geometry. At the atomic planes, the wave field amplitude is also nonzero, but in-between the planes it is by more than twice larger than the amplitude in the incidence wave. At the grazing incidence, the standing wave moves without noticeable change of the modulation contrast within a larger angular interval. At the steep incidence, the modulation contrast decreases much faster (compare the consequently thinner pink, violet, and blue lines in the left and right panels).

We turn to the case of nuclear scattering represented in the lower row of panels. The incident π-polarized wave excites the transition $-\frac{1}{2} \rightarrow -\frac{1}{2}$ between the nuclear sublevels in the ground and excited states. In this case, the distributions of the magnetic wave field $|\mathbf{H}_{tot}|$ in the space between the neighboring atomic planes are displayed. The distributions in the symmetric geometry are displayed in the central panel. The middle-thick green line represents the amplitude distribution in the crystal set at the Bragg angle. As well as in the case of electronic scattering, here the maximal contrast of the

amplitude distributions is reached. The nodes are located at the atomic planes. The antinodes between the planes have the doubled amplitude of the propagating wave. The difference to electronic scattering is the symmetric drop of the modulation contrast in the standing wave below and above the Bragg angle. Aside from that, the standing wave is shifting symmetrically to the left and to the right sides when the crystal is set off the Bragg position, as shown by the thickest orange and thinnest violet lines.

In the asymmetric geometry, the significant differences between the grazing and steep incidence are observed. At the side of grazing incidence, the contrast in modulation of the wave field amplitude drops down appreciably. On the contrary, at the side of the steep incidence the contrast characteristic for the symmetric case is preserved and maintained in a large angular range. This conclusion is also supported by the increase of the width of the reflection region for $|\beta| > 1$ as compared to the symmetric geometry (see the lower right-hand panel in Fig. 5). It is interesting that zero field value at the atoms at the Bragg angle is kept. From this observation one can conclude that the asymmetric mode with $|\beta| > 1$ turns out to be more advantageous from the point of view of the suppression of nuclear absorption in the crystal.

C. Penetration length and reflectivity

In the case of nuclear resonant scattering, the full reflectivity can be reached only in the Bragg position (see Sec. III D). Aside from this position, the reflectivity drops down due to

the rise of the nuclear excitation amplitude [see Fig. 4(b)], involving restoration of incoherent channels, particularly, of internal conversion. On the contrary, in electronic scattering the total reflectivity of the crystal $Q \sim 1$ is preserved within the finite angular range even at the angles, where the total field at the atomic planes is rather large [see the central panel in Fig. 4(a)] and, therefore, the photoelectronic absorption is restored. Quite an evident question arises as to why the reflectivity can be maintained at a high level under the condition of strong absorption of radiation by atoms. In order to clarify this issue, we consider the variation of the number of atomic centers participating in scattering in the angular range near the Bragg position. This number is directly related to the penetration length of radiation L_a into the crystal.

In the vicinity of the Bragg angle, a significant change of L_a can occur along with the strong modification of the wave field structure inside the crystal and, as a consequence, of the interaction conditions of radiation with atoms. Far off the Bragg angle, the penetration length is determined by the ordinary absorption of radiation by atoms due to photoelectric effect or due to internal electron conversion. But, within the limits of the reflection range, the decisive role starts to be played by the interference of the waves built up inside the crystal due to diffraction. The interference of the eigenwaves determines the structure of the wave field in the crystal space on both a small and large scale. As the result of the interference, the modulation of the total field amplitude arises with the period equal to the interplanar spacing, i.e., on the scale of several radiation wavelengths. In addition, the characteristic parameter of attenuation of the wave field amplitude changes on the scale essentially exceeding the wavelength.

The modulation of the field amplitude on a short scale was thoroughly discussed in previous sections. It takes place both for electronic and for nuclear scattering. However, in electronic scattering, due to the phase relations of the scattered waves, another specific kind of an interference occurs. This is a strong destructive interference between the waves propagating in the forward direction, the incident wave, and twice reflected one, occurring in a thin layer under the surface of the crystal. By this reason, within the finite angular interval the radiation is practically prevented from penetration into the crystal. *This interference damping of radiation is known as primary extinction.* The primary extinction determines a peculiar behavior of the damping parameter $\mathrm{Im}\varepsilon_0^{(2)}$. The angular dependence of $\mathrm{Im}\varepsilon_0^{(2)}$ is illustrated in Fig. 9. As one can see, due to the primary extinction in a wide angular interval, the following relation holds: $|\mathrm{Im}\varepsilon_0^{(2)}| \gg |\mathrm{Im}\chi_{00}/2|$. As a result, the damping of radiation in the crystal within this angular range appears to be much larger than that far off the Bragg region.

The primary extinction does not exist in the nuclear diffraction case. Here, only the short-range modulation of the wave field amplitude determines the angular variation of the damping parameter. The latter, starting from the value of $|\mathrm{Im}\eta/2|$ far off reflection range, goes to zero approaching the Bragg angle (see Fig. 9).

In order to characterize the length of penetration, we have to take into account that the wave field amplitude can be strongly modulated and, in addition, that the modulation pattern can move in space when the incidence angle changes
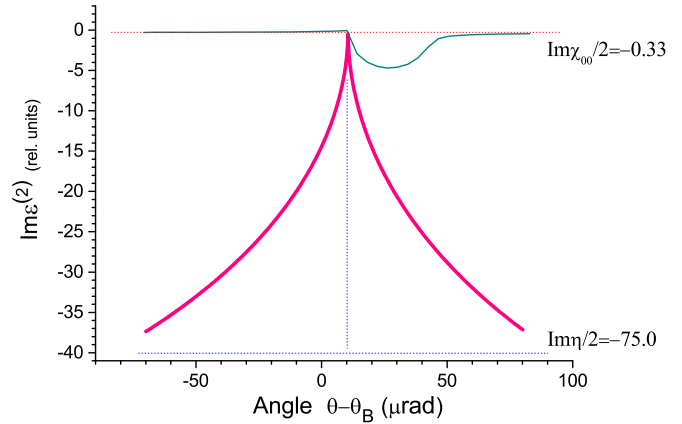
FIG. 9. Angular dependencies of the imaginary parts of $\varepsilon_0^{(2)}$ in the vicinity of the Bragg angle for electronic (the thin dark cyan line) and for nuclear (the thick pink line) scattering. Far off the Bragg angle, the limit values of $\mathrm{Im}\varepsilon_0^{(2)}$ are indicated at the right side.

within the reflection range (see Fig. 4). Therefore, the characteristic wave field amplitude should be averaged over the interplanar space. For the simplest model of the average, one can accept the half-sum of the amplitudes on the atomic plane and in the middle distance between the neighboring planes. For the (002) reflection of iron crystal, the phase factors for the mentioned positions are $\exp{(i\mathbf{Sr})} = \pm 1$, respectively. Then, for the scalar value of the averaged amplitude we obtain

$$E_{\text{averaged}} = E_0 \exp\left(K \, \mathrm{Im}\varepsilon_0^{(2)} L\right) \frac{1}{2}\left\{\left|1 - \frac{\beta \widetilde{\eta}_{10}}{2\varepsilon_0^{(1)} - \widetilde{\eta}_{00}}\right|\right.$$
$$\left. + \left|1 + \frac{\beta \widetilde{\eta}_{10}}{2\varepsilon_0^{(1)} - \widetilde{\eta}_{00}}\right|\right\}. \tag{18}$$

At the given susceptibility, the field attenuation on the path L is determined by the deviation of rays from the Bragg angle and by the asymmetry factor β. We define the length of penetration as a path L_a, within which the averaged amplitude drops by a factor of $\sqrt{e}$ (i.e., the averaged intensity of radiation after this path is $1/e$ of its initial value). At the end of the characteristic path L_a, the following relationship holds:

$$a = \exp\left(K \, \mathrm{Im}\varepsilon_0^{(2)} L_a\right) D, \tag{19}$$

where $a = \sqrt{1/e}$ and $D = \frac{1}{2}\{|1 - \frac{\beta \widetilde{\eta}_{10}}{2\varepsilon_0^{(1)} - \widetilde{\eta}_{00}}| + |1 + \frac{\beta \widetilde{\eta}_{10}}{2\varepsilon_0^{(1)} - \widetilde{\eta}_{00}}|\}$. To extract and calculate the value of L_a, it is necessary to take a logarithm of both parts of the equation. Finally, we arrive at

$$L_a = \frac{\lambda}{2\pi \, \mathrm{Im}\varepsilon_0^{(2)}} \ln\left[\frac{a}{D}\right]. \tag{20}$$

In Figs. 10(a) and 10(b), the angular dependencies of the penetration lengths for electronic and nuclear diffraction, respectively, are presented in vicinity of the Bragg angle for the various asymmetry factors. Far off the Bragg angle the normal absorption takes place, and L_a is $\approx 21 \, \mu$m in electronic scattering and only $\approx 0.1 \, \mu$m in nuclear scattering. In latter case, the penetration length is so small because of strong absorption in nuclear resonance.
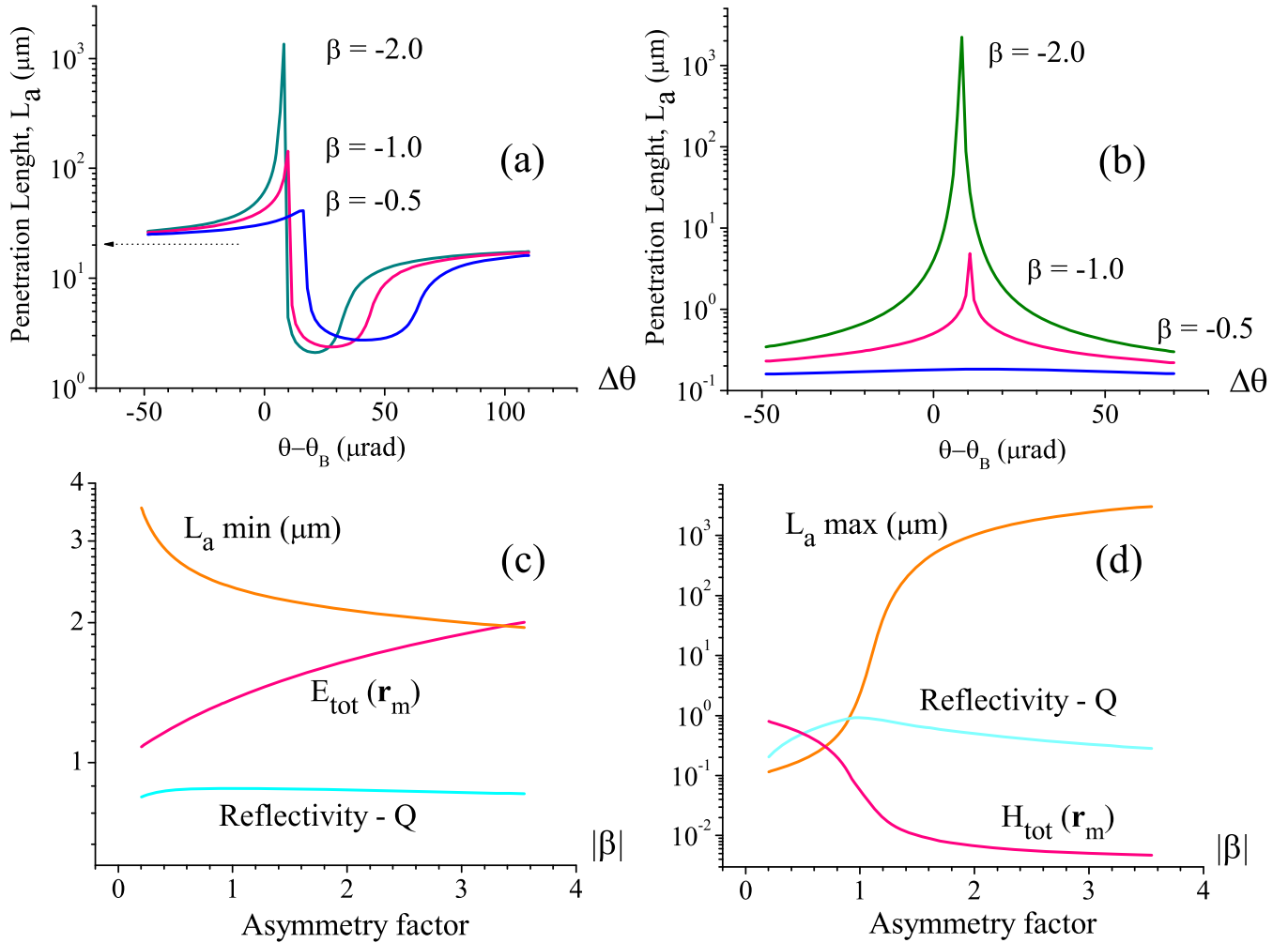
FIG. 10. In the upper row, the angular dependencies of the penetration length of radiation into the crystal are shown for the symmetric and asymmetric geometries of scattering with the values of the asymmetry factor $\beta = -0.5, -1.0$, and -2.0. In the lower row, the dependencies of the penetration lengths, amplitudes of the total fields, and reflectivities on the asymmetry factor are displayed for specific angular positions of the crystal [see the description of panels (c) and (d) in the text]. Panels (a) and (c) represent electronic scattering, and panels (b) and (d) represent nuclear scattering for the transition $-\frac{1}{2} \rightarrow -\frac{1}{2}$.

For two types of scattering, a drastic difference in the angular dependencies is immediately observed: a strong decrease of L_a within the clear-cut angular ranges for electronic scattering in contrast to a sharp rise of L_a, symmetrically extending on the entire region around the Bragg angle, for nuclear scattering. The dips in Fig. 10(a) occupy the distinct angular ranges, where the high reflectivity of radiation occurs [compare to the angular dependencies shown in Fig. 5(a)]. This is the primary extinction that causes such a behavior of L_a. Because of the primary extinction, the penetration length for the considered reflection turns out to be by approximately 10 times lesser than the regular value. In resonant nuclear scattering, the primary extinction does not take place. Therefore, the damping of radiation is caused only by the action of incoherent channels, among them, primarily, by internal conversion. Because by approaching the Bragg position the nuclear excitation amplitude at the atomic planes vanishes and incoherent channels are suppressed, the resonant radiation is allowed to penetrate deep into the crystal. Under the condition

of normally strong absorption in resonance, close to the Bragg angle L_a can reach thousands of microns, exceeding dramatically the regular penetration length far off the Bragg position [see Fig. 10(b)]. The anomalous penetration of radiation into the crystal is determined by the behavior of the damping parameter $\mathrm{Im}\varepsilon_0^{(2)}$. The angular dependencies of the damping parameter in the vicinity of the Bragg angle are displayed in Fig. 9.

The deep penetration also happens in electronic scattering, at the left edge of the high-reflectivity interval. However, the angular width of the L_a rise is extremely small in comparison to the width of the reflection region, because for x rays the real part of the scattering amplitude is always large in comparison to the imaginary part. Primary extinction, therefore, is the dominant reason for the high reflectivity in electronic scattering.

In Figs. 10(a) and 10(b), the angular dependencies are compared for three values of the asymmetry factor. Much stronger influence of the asymmetry on the values of L_a is

observed in nuclear resonant scattering. Whereas in electronic scattering the minimal values of L_a only slightly differ for $\beta = -0.5,\ -1.0,\ -2.0$, in nuclear resonant scattering for the same values of β the maximal values of L_a are different significantly (by several orders of magnitude).

In Figs. 10(c) and 10(d) the penetration lengths for specific angular positions are shown as functions of the asymmetry factor. The minimal and maximal values of the penetration lengths, L_a min and L_a max, are considered for electronic and nuclear scattering, respectively. In electronic scattering, the lengths L_a min correspond to the angular parameters α_c. In nuclear scattering, the lengths L_a max correspond to the angular positions $\theta - \theta_B = 0.5\ \mu$rad, i.e., to the very vicinity of the Bragg angle. They are compared to the total field amplitudes $E_{\text{tot}}(r_m)$ and $H_{\text{tot}}(r_m)$ at the scattering centers. Figures 10(c) and 10(d) show quite an opposite behavior of L_a in electronic and nuclear diffraction. When moving from the side of the grazing incidence $|\beta| < 1$ to the side of the steep incidence $|\beta| > 1$, the characteristic L_a and, hence, the number of the scattering centers N in the region of the high reflectivity decreases in electronic scattering and increases in nuclear scattering. The inverse behavior takes place for the total field amplitudes $E_{\text{tot}}(\mathbf{r}_m)$ and $H_{\text{tot}}(\mathbf{r}_m)$: the amplitude grows in electronic scattering and diminishes in nuclear scattering. By this reason, the reflectivity determined by the coherent sum of the amplitudes over the scattering centers $|N \times \mathbf{E}(r_m), \mathbf{H}(r_m)|^2$ stays at high level in electronic scattering and only slightly changes in nuclear scattering, as one can see in Figs. 10(c) and 10(d). Thus, in potential electronic scattering the decrease of the scattering centers number is compensated by growing of the total field amplitude at their positions, and vice versa: the decrease of the total field amplitude in resonant nuclear scattering is compensated by the increase of the number of scattering centers to maintain the high level of the reflectivity.

V. SUMMARY

A number of features distinguishes the elementary acts of interaction of resonant and nonresonant radiation with an atom. Potential scattering is characterized by the amplitude independent on the radiation frequency and, practically, it is a real value. Such kind of scattering is realized for the process of elastic scattering far away from an absorption edge. On the contrary, resonant scattering is characterized by the amplitude sharply dependent on the radiation frequency. Strictly in resonance, it is a pure imaginary value. Therefore, for γ radiation an ensemble of Mössbauer nuclei in a crystal represents a *resonating diffraction lattice. When a γ-ray photon is absorbed by the nuclear ensemble, a long-lived intermediate state is created.*

The entire process of scattering of a γ-ray photon by a nucleus can be divided into three stages: absorption of a primary photon with a formation of an intermediate excited state, dwelling in the intermediate state, and transition back to the ground state with an emission of a secondary photon. In the intermediate state, the nuclear excitation is delocalized, and a single photon is shared by all nuclei. This is how the scattering process exhibits a collective character. *By these features of nuclear excitation, the resonance diffraction of a*

γ-ray photon by an ensemble of nuclei should be considered as a macroscopic quantum phenomenon. In the photon diffraction process, the crystal behaves as a macroscopic quantum-mechanical object, the macroscopic quantum resonator. The collective state of nuclear excitation, called nuclear exciton, provides the physical basis for the use of a macroscopic polarization given by the Maxwell equations to treat the radiative effects of nuclei.

The probability of an internal electronic conversion in scattering at an individual nucleus is so large, that the localization of excitation with the loss of photon is very likely. And yet the coherence of the collective response of nuclei in a crystal permits the radiative channel not only to survive, but even to become dominant in the process of an interaction of a γ-ray photon with a nuclear array. When the Bragg requirements are satisfied, the excited atomic currents contribute to the field, and the constructive interference of the waves emitted by atoms gives rise to the formation of the strong waves in some directions.

In this work, as the thought experiment the diffraction of radiation in the crystal of iron entirely consisting of the nuclear resonant isotope ^{57}Fe was considered for the (002) Bragg reflection. The angular dependencies of the reflection coefficient for electronic and nuclear scattering in the vicinity of Bragg reflection were computed and displayed on the complex plane (see Fig. 2). The specific R contours were obtained for electronic and nuclear scattering. The total amplitude of the electromagnetic field was directly evaluated.

The structure of the total field in the space between the neighboring reflecting atomic planes can be strongly modified due to diffraction. The field amplitude is modulated in the direction orthogonal to the scattering planes (see Fig. 4). The drop of the total field amplitudes at the atomic planes at the Bragg angle to zero corresponds to the Borrmann effect in electronic scattering and to the Kagan-Afanas'ev effect in nuclear scattering. While for realization of the Borrmann effect the disappearance of the fields at the atoms is a necessary condition, for the Kagan-Afanasev effect it is optional. Due to diffraction, in the case of an excitation of the nuclear transition with the change of the magnetic number $|\Delta M| = 1$ the circularly polarized total magnetic field at the nuclei is created. At the same time, the magnetic moment of the nuclear transition appears to be also circularly polarized, but in the opposite direction of rotation (see Fig. 3). Therefore, tuned to excite the given nuclear transition, the total field created in diffraction by the nuclear ensemble is not able to produce the excitation of nuclei when approaching the Bragg angle. This is a very typical situation for the Kagan-Afanasev effect: the field at nuclei is not zero, but the interaction with the nuclei is suppressed.

The main reason for the high reflectivity in nuclear scattering is the suppression of all inelastic channels. One should then conclude that the entire reflection takes place under conditions, where the excitation amplitude becomes zero. How can these facts can be reconciled? The question concerns the entire absorption and reflection of the wave field in the crystal. They are determined by the total number of nuclei involved in diffraction: $N \sim 1/\sqrt{\alpha}$, where α is an angular parameter proportional to the deviation from the Bragg angle, and by the field amplitude at the positions of the nuclei:

$\mathbf{H}(\mathbf{r}_m) \sim \sqrt{\alpha}$. Dropping down of the field amplitude is accompanied by growing up with the same tempo of the number of reflecting centers. When absorption is considered, the contributions of all nuclei are summed incoherently. Then, the entire absorption turns out to be proportional to $N \times |\mathbf{H}(\mathbf{r}_m)|^2 \sim (1/\sqrt{\alpha})\alpha = \sqrt{\alpha}$, i.e., it disappears when approaching the Bragg angle. When diffraction is considered, the contributions of all nuclei are summed coherently. Then, the reflection is the square of the summary scattering amplitude $|N \times \mathbf{H}(\mathbf{r}_m)|^2 \sim |(1/\sqrt{\alpha})\sqrt{\alpha}| = 1$. In spite of the vanishing wave field when approaching the Bragg position, reflection does not vanish. In contrast, it becomes total at the Bragg position. Thus, we see that coherent scattering of all nuclei is able to maintain diffraction, even though the field amplitude at the place of each individual nucleus vanishes.

The asymmetry in scattering geometry reveals itself in different way in electronic and nuclear scattering. Several characteristics of Bragg scattering were analyzed in dependence of the asymmetry factor $\beta = -\sin\theta_0 / \sin\theta_1$, where θ_0 and θ_1 are glancing angles of the incident and reflected beams. In electronic and nuclear scattering, the maximal value $|R|_m$ of the reflection coefficient and the width $|R|_w$ of its angular dependence vary differently with the asymmetry parameter β (see Fig. 6). In electronic scattering, when moving from the side of the grazing incidence to the side of the steep incidence $|R|_m$ grows monotonously, and it can become much higher than unity. That is, the amplitude of the reflected wave can significantly exceed that of the incident wave. The width $|R|_w$ in this case gradually falls. In nuclear scattering, $|R|_m$ reaches saturation at the level of unity soon after the symmetry point $\beta = -1$. As far as $|R|_w$ is concerned, it significantly exceeds the corresponding width of the diffraction region in electronic scattering, by more than one order of magnitude. In contrast to electronic scattering, the width in nuclear scattering reaches minimum at the symmetric position, and it rises with deviation from this position to both sides.

The distributions of the wave field amplitudes in the space between the neighboring atomic planes were computed for the asymmetry factors $\beta = -0.5, -1, -2.0$ (see Fig. 8). Strong spatial modulation of the amplitude is observed in the Bragg angle region. In nuclear scattering, the modulation in the wave field amplitude falls down below and above the Bragg angle symmetrically, in contrast to electronic scattering. When passing to the asymmetric reflection in the grazing incidence case, the contrast of the modulation decreases appreciably. On the contrary, at the side of the steep incidence, the contrast characteristic for the symmetric case is preserved and maintained in a large angular range. Aside from that, at the Bragg angle the zero value of the field at the atoms is kept.

A drastic difference is observed in the angular dependencies of the penetration lengths for two types of scattering: a strong decrease of L_a within the range of the high reflectivity for electronic scattering, in contrast to a great increase of L_a, spreading over the entire region around the Bragg angle, for nuclear scattering (see Fig. 10). This behavior of L_a is caused by the interference of the waves formed inside the crystal under the conditions of coherent scattering. The interference damping of radiation in electronic scattering is known as primary extinction. In resonant nuclear scattering, the primary extinction is absent. Therefore, the damping of radiation is caused only by the action of incoherent channels, mostly by internal electron conversion. Since in approaching the Bragg position the nuclear excitation amplitude vanishes and the incoherent channels are suppressed, the resonant radiation is allowed to penetrate deep into the crystal.

When passing from the case of the grazing incidence $|\beta| < 1$ to the case of the steep incidence $|\beta| > 1$, in the region of the high reflectivity the penetration length L_a and, hence, the number of scattering centers N decreases in electronic scattering and increases in nuclear scattering. Thus, in potential electronic scattering the decrease of the scattering centers number is compensated by growing of the total field amplitude at their positions, and vice versa: the decrease of the total field amplitude in resonant nuclear scattering is compensated by the increase of the number of scattering centers to maintain the high level of reflectivity.

In this paper we did not touch some other specific features of nuclear diffraction, particularly, its energy and time dependence, and, especially, the strong polarization dependence of the magnetic and electric fields structure inside the crystals. Due to the polarization dependence, it became possible to obtain a pure nuclear diffraction without any contribution of coherent electronic scattering [21]. In particular, the polarization dependence of the field structure in combination with the existence of the nuclear states mixed in the spin projections for the $FeBO_3$ crystal allowed for the creation of the Synchrotron Mössbauer Source, which presents the source of coherent nuclear resonant γ radiation of the ^{57}Fe isotope [22–26].

[1] W. Friedrich and P. Knipping, Sitz. Ber. Bauer. Akad. Wiss., 311 (1912).

[2] P. J. Black and I. P. Duerdoth, Proc. Phys. Soc. (London) **84**, 169 (1964).

[3] R. L. Mössbauer, Z. Phys. **151**, 124 (1958); Naturwiss. **45**, 538 (1958).

[4] G. T. Trammell, in *Proceedings of the International Atomic Energy Agency Symposium on Chemical Effects of Nuclear Transformations, Prague 1960* (IAEA, Vienna, 1961), Vol. 1, p. 75.

[5] A. M. Afanas'ev and Yu. Kagan, Pis'ma Zh. Eksp. Teor. Fiz. **2**, 130 (1965) (in Russian) [JETP Lett. **2**, 81 (1965)].

[6] G. V. Smirnov, Hyperfine Interact. **27**, 203 (1986).

[7] P. P. Ewald, Ann. Phys. **49**, 1 (1916); **49**, 117 (1916); **54**, 519 (1917); Acta Crystallogr. **11**, 888 (1958).

[8] Yu. Kagan, A. M. Afanas'ev, and I. P. Perstnev, Zh. Eksp. Teor. Fiz. **54**, 1530 (1968) (in Russian) [J. Exp. Theor. Phys. **27**, 819 (1968)].

[9] G. V. Smirnov and A. I. Chumakov, Zh. Eksp. Teor. Fiz. **89**, 1169 (1985) (in Russian) [J. Exp. Theor. Phys. **62**, 673 (1985)].

[10] Z. G. Pinsker, *Dynamical Scattering of X Rays in Crystals*, Springer Series in Solid State Sciences (Springer, Berlin, 1978), Vol. 3.

[11] A. M. Afanas'ev and Yu. M. Kagan, Zh. Eksp. Teor. Fiz. **48**, 327 (1965) (in Russian) [J. Exp. Theor. Phys. **21**, 215 (1965)].

[12] U. van Bürck, G. V. Smirnov, R. L. Mössbauer, F. Parak, and N. A. Semioschkina, J. Phys. C: Solid State Phys. **11**, 2305 (1978).

[13] G. Borrmann, Phys. Z. **42**, 157 (1941); Z. Phys. **127**, 297 (1950).

[14] B. W. Battermann and H. Cole, Rev. Mod. Phys. **36**, 681 (1964).

[15] G. V. Smirnov, U. van Bürck, and R. L. Mössbauer, J. Phys. C: Solid State Phys. **21**, 5835 (1988).

[16] M. V. Kovalchuk and V. G. Kohn, Uzpekhi Fizicheskikch Nauk **149**, 69 (1986) (in Russian) [Sov. Phys. Usp. **29**, 426 (1986)].

[17] J. Zegenhagen and A. Kazimirov, *X-ray Standing Wave Technique, Principles and Applications*, Series an Synchrotron Radiation Techniques and Applications Vol. 7 (World Scientific, Singapore, 2013).

[18] Yu. Kagan and A. M. Afanas'ev, Z. Naturforsch. **28a**, 1351 (1973).

[19] U. van Bürck, G. V. Smirnov, R. L. Mössbauer, H. J. Maurus, and N. A. Semioschkina, J. Phys. C: Solid State Phys. **13**, 4511 (1980).

[20] Yu. Kagan and A. M. Afanas'ev, Zh. Eksp. Teor. Fiz. **49**, 1504 (1965) (in Russian) [J. Exp. Theor. Phys. **22**, 1032 (1966)].

[21] G. V. Smirnov, V. V. Sklyarevskii, R. A. Voscanyan, and A. N. Artem'ev, Pis'ma Zh. Eks. Teor. Fiz. **9**, 123 (1969) (in Russian) [JETP Lett. **9**, 70 (1969)].

[22] G. V. Smirnov, U. van Bürck, A. I. Chumakov, A. Q. R. Baron, and R. Rüffer, Phys. Rev. B **55**, 5811 (1997).

[23] G. V. Smirnov, Hyperfine Interact. **125**, 91 (2000).

[24] T. Mitsui, M. Seto, S. Kikuta, N. Hirao, Y. Ohishi, H. Takei, Y. Kobayashi, S. Kitao, S. Higashitaniguchi, and R. Masuda, Jpn. J. Appl. Phys. **46**, 821 (2007).

[25] G. V. Smirnov, A. I. Chumakov, V. B. Potapkin, R. Rüffer, and S. L. Popov, Phys. Rev. A **84**, 053851 (2011).

[26] V. Potapkin, A. I. Chumakov, G. V. Smirnov, J. P. Celse, R. Rüffer, C. McCammon, and L. Dubrovinsky, J. Synchrotron Radiat. **19**, 559 (2012).